CZECH TECHNICAL UNIVERSITY
FACULTY OF NUCLEAR SCIENCES AND PHYSICAL ENGINEERING

REVIEW WORK

Present status of neutrino physics

Jiří Bočan

Supervisor: Ing. Ivan Štekl, CSc.

CTU Prague
September 2003

Acknowledgement

Firstly, I would like to thank Ivan Štekl from the Institute of Experimental and Applied Physics, Czech Technical University in Prague, for introducing me into the neutrino physics and for having conducted and supervised my review work, as well as for his advice, help and support.

Next, I would like to express my gratitude to Professor Claude Leroy from the University of Montréal for his constant and useful help.

My thanks also go to Professor Jiří Tolar from the Faculty of Nuclear Sciences and Physical Engineering, Czech Technical University in Prague, for his contribution.

Finally, the biggest thanks and my highest gratitude are dedicated to my parents for their full support, encouragement and understanding.

Thank you!

Contents

List of Figures

List of Tables

Introduction

This work describes the present status of the neutrino physics. The text is divided into six chapters and two appendices.

The main parts treat of the fundamental neutrino properties, the double beta decay, the phenomenon of neutrino oscillation, as well as the atmospheric, solar and supernova neutrinos. Each chapter includes a theoretical part providing the basic knowledge and theory, and the experimental part discussing the methods and principles of how to measure and to prove the theoretical predictions. The most important projects of the neutrino physics are also described in details.

Finally, the review work contains two appendices. The first one summarizes the experiments associated with neutrinos giving the basic information about them. The second appendix gives a short historical survey of the neutrino physics.

Chapter 1

Neutrino properties

Neutrinos are electrically neutral fermions (particles of spin 1/2). Today, three species (flavors) of neutrinos are known [1]: the electron neutrino ν_e, the muon neutrino ν_μ, the recently discovered tau neutrino ν_τ and their antiparticles $\bar{\nu}_e$, $\bar{\nu}_\mu$, $\bar{\nu}_\tau$. Theoretically, it is possible that a fourth "sterile" neutrino ν_s exists (more in Chapter 3, page 20).

Electron neutrinos are produced in the nuclear $\beta^\pm$-decays [2]:

$$\beta^-: \ A(Z,N) \rightarrow A(Z+1,N-1) + e^- + \bar{\nu}_e, \tag{1.1}$$

$$\beta^+: \ A(Z,N) \rightarrow A(Z-1,N+1) + e^+ + \nu_e, \tag{1.2}$$

in the neutron decay $n \rightarrow p + e^- + \bar{\nu}_e$, as well as in the decays of mesons (π, K, D, B), baryons (Λ, Σ, Ξ, Ω) or leptons (μ, τ) [3]. But the basic processes producing ν_e and $\bar{\nu}_e$ are lying in the quark transitions [2]:

$$d \rightarrow u + e^- + \bar{\nu}_e, \tag{1.3}$$

$$u \rightarrow d + e^+ + \nu_e. \tag{1.4}$$

Muon neutrinos are produced mostly in decays of the same kinds of particles as in the case of electron neutrinos [3]. Finally, tau neutrinos are the products of decays of tau lepton and several sorts of mesons or baryons, too.

Neutrinos of each flavor [2] participate in the reactions, which are mediated by the gauge bosons $W^\pm$. These "charged current" (CC) reactions involve the processes $W^\pm \rightarrow a^\pm + \nu_a(\bar{\nu}_a)$, where $a = e, \mu, \tau$. Neutrinos can also participate in "neutral current" (NC) reactions mediated by Z^0 boson (mainly elastic or quasielastic scattering processes). Decays $Z^0 \rightarrow \nu_a + \bar{\nu}_a$ have not been detected, yet.

1.1 Measurement of neutrino mass

To solve this difficult problem, many methods have been invented, but at the present, the suitable and usable ones are the direct kinematic searches (β-, π- or τ-decay), the double beta decay studies (see Chapter 2), and the neutrino oscillations (see Chapter 3) giving the differences between squared masses of two neutrinos of different flavors.

1.1.1 β-decay

Up to now, the direct kinematic measurements of the neutrino mass produce only upper limits. The most sensitive searches have been associated with $\bar{\nu}_e$, where the kinematic endpoint of the outgoing electron spectrum of the tritium decay process

$$^3\mathrm{H} \rightarrow {}^3\mathrm{He} + e^- + \bar{\nu}_e \tag{1.5}$$

is analysed (Kurie plot). There is no necessity in the kinematic measurements to use the theoretical calculations as in the $\beta\beta$-decay (where the results depend on the nuclear matrix element calculations). The shapes of electron spectra are analytically described by [2, 4, 5]:

$$m_\nu = 0: \quad N_e(E) \propto F(Z,E)\sqrt{E^2 - m_e^2}\, p_e\, E\, (Q-E)^2, \tag{1.6}$$

$$m_\nu \neq 0: \quad N_e(E) \propto F(Z,E)\sqrt{E^2 - m_e^2}\, p_e\, E\, (Q-E)\sqrt{(Q-E)^2 - m_\nu^2}, \tag{1.7}$$

where $F(E,Z)$ is the Fermi function describing the Coulomb interaction between the emitted electron and the nucleus in the final state, Q is the energy release (Q-value[1]), p_e and m_e are the momentum and the mass of electron, respectively. The number of electrons in an energy interval ΔE near the Q-value is proportional to [6]:

$$n(Q-\Delta E) \propto \left(\frac{\Delta E}{Q}\right)^3. \tag{1.8}$$

It implies that nuclides with small Q-value are advantageous, but even for tritium with the relatively low endpoint energy of about $Q_{^3\mathrm{H}} \approx 18.6$ keV only about one billionth of all electrons lies in a region of 20 eV below the endpoint. The so-called Kurie plot used for analysing the electron spectrum is given by [2]: $K(E) \equiv \sqrt{N(E)/[F(Z,E)p_eE]}$; the shape dependence of the electron spectrum (see Figure 1.1) is distinct for massless and massive neutrino ($m_\nu = 0 \Rightarrow$ abscissa, $m_\nu \neq 0 \Rightarrow$ dashed curve).

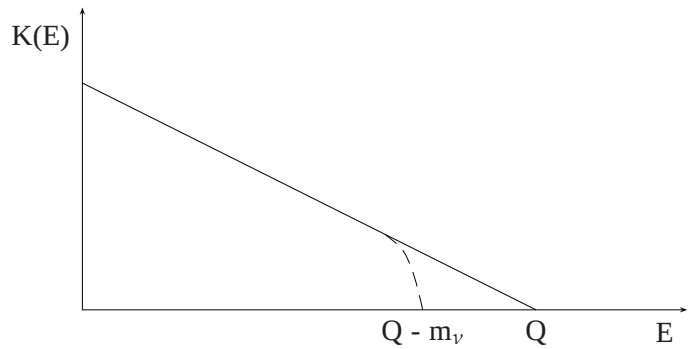

Figure 1.1: Kurie plot, ref. [2].

The actual limits achieved by this method are (CL = Confidence level) [3, 4, 7]:

$$m_{\nu_e} < 2.2 \text{ eV at 95\% CL (Troisk)},$$
$$m_{\nu_e} < 2.2 \text{ eV at 95\% CL (Mainz)},$$
$$\boldsymbol{m_{\nu_e} < 3.0 \text{ eV at 95\% CL (PDG)}},$$

when Mainz experiment used frozen molecular tritium condensed on a graphite substrate and Troisk experiment used gaseous molecular tritium source [4]. The Particle Data Group (PDG) limit is a general compilation of the different experimental results.

The KATRIN collaboration [8] involving previous experimental groups in Mainz and Troisk has been formed to perform a next-generation experiment scaling up the size of

[1]The Q-value for the reaction $X \rightarrow Y + e^- + \bar{\nu}_e$ is given by $Q = [m(X) - m(Y) - m(e^-) - m(\bar{\nu}_e)]c^2$.

previous experiments. This experiment uses a much more intense tritium source and would reach a sensitivity down to 0.2 eV mass.

However, all these experiments show some excess in the number of electrons near the endpoint of the spectrum rather than the deficiency expected if $m_\nu \neq 0$. This experimental fact is caused by some unknown systematic effect [2]. That is the reason, why the Particle Data Group [3] recommends values derived from different experiments as an average of the best and the most reliable results.

1.1.2 π-decay

The muon neutrino mass can be measured by the detailed study of the muon spectrum from the charged pion decays [2, 4, 5]:

$$\pi^\pm \to \mu^\pm + \nu_\mu(\bar{\nu}_\mu), \tag{1.9}$$

while the ν_μ mass (for π^+) is given by [4]:

$$m^2_{\nu_\mu} = m^2_{\pi^+} + m^2_{\mu^+} - 2m_{\pi^+}\sqrt{p^2_{\mu^+} + m^2_{\mu^+}}, \tag{1.10}$$

where p_{μ^+} is the muon momentum, m_{π^+} and m_{μ^+} the pion and muon masses, respectively. The value of m_{ν_μ} is quite uncertain as a result of its dependence on m_{π^+} (see ref. [3, 4] for m_{π^+} values). The best limits, at present, are [2, 3]:

$$m_{\nu_\mu} < 170 \text{ keV at 90\% CL (PSI)},$$
$$\boldsymbol{m_{\nu_\mu} < 190 \text{ keV at 90\% CL (PDG)}}.$$

1.1.3 τ-decay

For determination of the tau neutrino mass the following lepton decays are used [3, 4, 5]:

$$\tau^- \to 2\pi^- + \pi^+ + \nu_\tau, \tag{1.11}$$
$$\tau^- \to 3\pi^- + 2\pi^+ + \nu_\tau\ (+\pi^0). \tag{1.12}$$

The current limit is [3]:

$$\boldsymbol{m_{\nu_\tau} < 18.2 \text{ MeV at 95\% CL (ALEPH - (1.12), PDG)}}.$$

1.2 Dirac and Majorana neutrinos, chirality and helicity

One of the unsolved problems about neutrinos is, whether neutrino is identical to its antiparticle (Majorana case) or whether neutrino and antineutrino are two different ones (Dirac case; like quarks or charged leptons) [2, 6, 9].

It is experimentally observed that neutrinos emitted in β^--decay ($\bar{\nu}_e$'s) cannot be captured in reaction caused by ν_e's [2]:

$$\bar{\nu}_e + {}^{37}\mathrm{Cl} \not\to {}^{37}\mathrm{Ar} + e^-, \tag{1.13}$$
$$\nu_e + {}^{37}\mathrm{Cl} \to {}^{37}\mathrm{Ar} + e^-. \tag{1.14}$$

But that is not a proof of the neutrino character. This question seems to be answered only by the neutrinoless double beta decay search [2].

The reason is that the weak interaction (the way how neutrinos interact) is chiral (something is chiral, when it is not superposable to its mirror image [9]) and only neutrinos

of left-handed chirality can be detected through the reaction (1.14) [2]. The right-handed antineutrinos have the "wrong" chirality and cannot be detected by this way (this is called "chiral prohibition"). But if neutrinos are massive, the chirality is not a good quantum characteristic, because a very small possibility exists that reaction (1.13) is feasible [2].

Another quality of the particles is their helicity [2, 9]. One of the main properties of a particle is its spin representing a particle self-rotation. If a projection of the spin on the particle velocity direction is opposite to it, the particle is of left helicity, and of right helicity velocity and projection of the spin are in the same direction.

The weak interaction produces only left-handed chirality particles. If $m_\nu = 0$, that means, the particle is left-handed; if $m_\nu \neq 0$, this implication is not valid [9].

1.3 Observability and sources of neutrinos

As Bethe and Peierls, in 1934, calculated the values of the interaction cross section of the reactions $\nu + n \rightarrow e + p$ and $\bar{\nu} + p \rightarrow e^+ + n$, it seemed to be impossible to catch neutrinos on Earth; for neutrino energy of 1 MeV the cross section values are less than 10^{-43} cm^2 only. The practical consequences [2, 9] of so small cross sections are, for example, that the free path of 1 MeV neutrino in lead is about one light year, or if a beam of 10^{10} neutrinos heads toward Earth, all but one would emerge on the other side, or that during each thousand years, only one of all neutrinos can interact with a human body. That all means that for detection of these particles, large detectors and/or powerful sources producing very intensive neutrino beams are needed.

One of the most powerful neutrino sources [2] is our Sun that emits about 2×10^{38} neutrinos per second, leading to a flux at the Earth surface of 6×10^{10} cm^{-2}s^{-1} with the energy $E \leq 0.42$ MeV, and about 5×10^6 cm^{-2}s^{-1} with energy 0.8 MeV $\leq E \leq$ 15.0 MeV. Nuclear power plants produce electron antineutrinos. 3 GW plant emits about 7.7×10^{20} electron antineutrinos of the energy of several MeV per second, creating a flux of approximately 6×10^{11} cm^{-2}s^{-1} at 100 m. At remote locations the average $\bar{\nu}_e$ number density created by all nuclear power plants on Earth is about $10^6 - 10^7$ cm^{-3}. The relic neutrino number density is about 110 cm^{-3} for each neutrino flavor with a black-body spectrum with the average energy of 5×10^{-4} eV. Earth natural radioactivity flux is roughly 6×10^6 cm^{-2}s^{-1} (number density of 2×10^{-4} cm^{-3}) of neutrino energy $E \leq 1$ MeV. The flux of the atmospheric neutrinos at the Earth surface is $\sim 10^{-1}$ cm^{-2}s^{-1}. Finally, the very sporadic but much more important sources of neutrinos are the Type II supernovae (more in Chapter 6) emitting about 6×10^{58} neutrinos and antineutrinos for several seconds with typical energies $E \leq 30$ MeV. All these neutrino source characteristics are summarized in Table 1.1.

Neutrino source	$\langle E \rangle$ (MeV)	ϕ (cm^{-2}s^{-1})	ρ (cm^{-3})
Sun	≤ 0.42	6×10^{10}	
	0.8 – 15.0	5×10^6	
Nuclear power plant (3 GW)	1-5	6×10^{11} (at 100 m)	$10^6 - 10^7$ (in total)
Relic neutrinos	5×10^{-4}		110 (each flavor)
Earth natural radioactivity	≤ 1	6×10^6	2×10^{-4}
Atmospheric neutrinos		10^{-1}	
Supernova neutrinos	≤ 30		

Table 1.1: The neutrino source characteristics. The average energy $\langle E \rangle$, the flux ϕ and the numerical density ρ of the neutrinos on the surface of Earth are listed, ref. [2].

Chapter 2

Double beta decay

The double beta decay ($\beta\beta$) is a very important process in nuclear and particle physics. It appears, when the ordinary single β-decay is energetically forbidden or strongly suppressed by the large angular momentum differences between the initial and final states (e.g. ^{48}Ca $\rightarrow$ ^{48}Sc). $\beta\beta$-decay is a process of the second order Fermi theory converting a nucleus $A(Z, N)$ into an isobar with the electric charge differing by two units. The corresponding decay rates are too low; a typical lifetime of the nuclei liable to $\beta\beta$-decay is $T \gtrsim 10^{18}$ years. The typical energy release (Q-value) for $\beta\beta$-decay is about several MeV [2, 6, 10].

At a fundamental level, $\beta\beta$-decay is the transition of two d quarks into two u quarks or vice versa [2]. The basic types of $\beta\beta$-decay (marked as $2\nu\beta\beta$-decays because of the emission of two neutrinos) are the following [10]:

- two electron capture (EC/EC):

$$2e^- + A(Z, N) \rightarrow A(Z-2, N+2) + 2\nu_e, \tag{2.1}$$

- electron capture with emission of positron (β^+/EC):

$$e^- + A(Z, N) \rightarrow A(Z-2, N+2) + e^+ + 2\nu_e, \tag{2.2}$$

- two positron emission ($\beta^+\beta^+$):

$$A(Z, N) \rightarrow A(Z-2, N+2) + 2e^+ + 2\nu_e, \tag{2.3}$$

- two electron emission ($\beta^-\beta^-$):

$$A(Z, N) \rightarrow A(Z+2, N-2) + 2e^- + 2\bar{\nu}_e. \tag{2.4}$$

The $\beta^+\beta^+$-decays are always accompanied by EC/EC or β^+/EC processes [6]. Their rate is small and energetically only possible for six nuclides. The predicted $\beta^+\beta^+$-decay half-lives are of the order of $10^{25} - 10^{26}$ years, while in the case of β^+/EC it is only about 10^{22} years and for EC/EC it is on the level 10^{20} years. Thus, it gives more chance to observe EC/EC or β^+/EC channels. But up to now, the experimental effort is concentrated to $\beta^-\beta^-$ processes.

Generally, $2\nu\beta\beta$ processes conserve electric charge and lepton number and they are, as well, permitted in the Standard Model (SM) of particle physics [2]. Several characteristics of some nuclides (the Q-value ($Q_{2\nu\beta\beta}$), half-life ($T_{1/2}^{2\nu\beta\beta}$) and the natural abundance (A_N) of each nuclide) are listed in Table 2.1.

Isotope	$Q_{2\nu\beta\beta}$ (keV)	$T^{2\nu\beta\beta}_{1/2}$ (yr)	A_N (%)
^{48}Ca	4,271.0	$4.20^{+2.10}_{-1.00} \times 10^{19}$	0.19
^{76}Ge	2,039.6	$1.43^{+0.09}_{-0.07} \times 10^{21}$	7.80
^{82}Se	2,995.0	$(0.90 \pm 0.10) \times 10^{20}$	9.40
^{96}Zr	3,350.0	$2.10^{+0.80}_{-0.40} \times 10^{19}$	2.78
^{100}Mo	3,034.0	$(8.00 \pm 0.70) \times 10^{18}$	9.63
^{116}Cd	2,802.0	$3.30^{+0.40}_{-0.30} \times 10^{19}$	7.49
^{128}Te	868.0	$(2.50 \pm 0.40) \times 10^{24}$	31.69
^{130}Te	2,533.0	$(0.90 \pm 0.15) \times 10^{21}$	33.80
^{150}Nd	3,367.1	$(7.00 \pm 1.70) \times 10^{18}$	5.64
^{238}U	1,145.8	$(2.00 \pm 0.60) \times 10^{21}$	99.27

Table 2.1: The $2\nu\beta\beta$-decay nuclides, ref. [10, 11].

Besides the $2\nu\beta\beta$ processes, another decay given by:

$$A(Z, N) \rightarrow A(Z \pm 2, N \mp 2) + 2e^{\mp}, \tag{2.5}$$

so-called "neutrinoless" double beta decay ($0\nu\beta\beta$), is predicted and intensively searched for. In this case, neutrino or antineutrino emitted in one of the elementary β-decay processes forming $\beta\beta$-decay can be absorbed in another one. As the consequence, the lepton number is not conserved. In addition, since the absorbed ν or $\bar{\nu}$ has a wrong chirality, $0\nu\beta\beta$-decay breaks the chirality conservation [2].

Although this decay is forbidden by SM, in extended models some exotic modes of $0\nu\beta\beta$ are possible [6]. For example $0\nu\beta\beta$ with emission of Majoron ($0\nu(2)\chi\beta\beta$) given by:

$$A(Z, N) \rightarrow A(Z + 2, N - 2) + 2e^{-} + (2)\chi. \tag{2.6}$$

Majoron χ is the Goldstone-boson of a spontaneous breaking of a global lepton-number symmetry, whose theoretical singlet, doublet and triplet models, as well, exist depending on its transformation properties. Experimentally (LEP [1]), triplet and pure doublet models are excluded because they would contribute 2 (triplet) or 0.5 (doublet) neutrino flavors [6].

Several new Majoron models developed during the 90th of the last century predicting the different shapes for the set of electron spectra (see Figure 2.1) written as:

$$\frac{\mathrm{d}N}{\mathrm{d}E} \propto (Q - E)^n F(E, Z), \tag{2.7}$$

where Q represents the Q-value of decay, $F(E, Z)$ is the Fermi function and n is the spectral index ($n = 1$ represents the classical Majorons, $n = 3$ lepton number carrying Majorons, $n = 5$ is used for $2\nu\beta\beta$-decay and $n = 7$ for other Majoron models) [6].

The half-life limits for $0\nu(2)\chi\beta\beta$ ($n = 1$) together with the corresponding effective Majorana masses are shown in Table 2.2. The experimental values for $n = 3$ and $n = 7$ were obtained from Heidelberg-Moscow experiment [6, 12, 13, 14]:

$$T^{0\nu\chi}_{1/2} > 5.85 \times 10^{21}\text{yr}\ (n = 3),\ T^{0\nu\chi}_{1/2} > 6.64 \times 10^{21}\text{yr}\ (n = 7).$$

In the year 2001, the first evidence of $0\nu\beta\beta$-decay was published by Heidelberg-Moscow experiment [13, 14]. The measured half-life is $T^{0\nu\beta\beta}_{1/2} = (0.8 - 18.3) \times 10^{25}$ yr (95 % CL) implying the value of the effective neutrino mass $\langle m_\nu \rangle = (0.11 - 0.56)$ eV (95 % CL); the best values are 1.5×10^{25} yr and 0.39 eV. As this result is the first, it is very controversial.

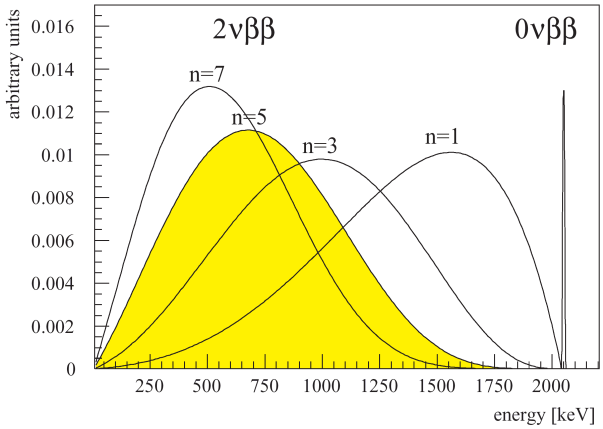

Figure 2.1: The $0\nu(2)\chi\beta\beta$-decay modes, ref. [6].

Isotope	$T_{1/2}^{0\nu\beta\beta}$ (yr)	Author/Experiment
^{48}Ca	$> 1.8 \times 10^{22}$	Ogawa *et al.*
^{76}Ge	$\approx 1.5 \times 10^{25}$	Heidelberg-Moscow
	$> 1.57 \times 10^{25}$	IGEX
^{100}Mo	$> 5.5 \times 10^{22}$	ELEGANT-V
	$> 4.9 \times 10^{21}$	Liquid Ar ionization chamber (Gran Sasso)
^{116}Cd	$> 1.7 \times 10^{23}$	^{116}Cd Solotvina experiment
	$> 2.9 \times 10^{21}$	ELEGANT-V
^{128}Te^{geo}	$> 7.7 \times 10^{24}$	Bernatowitz *et al.*
^{130}Te	$> 2.1 \times 10^{23}$	MIBETA
^{136}Xe	$> 7.0 \times 10^{23}$	Belli *et al.*
	$> 4.4 \times 10^{23}$	TPC (Gotthard underground laboratory)
	$> 4.5 \times 10^{23}$	DAMA liquid Xe scintillator (Gran Sasso)

Table 2.2: The compilation of the results of $0\nu\beta\beta$-decay measurements, ref. [11, 14, 15, 16].

A reason of the importance of the search for $0\nu\beta\beta$-decay is, that it would prove Majorana character of neutrinos with finite masses having an origin beyond SM. Problems with the determination of the exact value of the effective Majorana neutrino mass $|\langle m \rangle|$ are related with values of the elements of the nuclear matrix of $0\nu\beta\beta$-decay, which are only approximately known. Half-life of $0\nu\beta\beta$ is given by:

$$(T_{1/2}^{0\nu\beta\beta})^{-1} = A\left(\frac{\langle m_{\nu_e} \rangle}{m_e}\right)^2,$$

where the factor A includes, by the way, the nuclear matrix elements, and m_e is the electron mass.

2.1 Experimental status

2.1.1 Experiment types

The $\beta\beta$-decay half-lives are in the order of $10^{18} - 10^{26}$ years. It implies that $\beta\beta$-processes are very rare. To achieve experimental results, the precise low-level counting techniques are required. For such measurement, the highly isotopical enriched materials with high Q-value and a background (given in counts/year/kg/keV) as low as possible are needed.

The main background sources are the cosmic ray muons, the man-made ^{137}Cs, the products of natural decay chains of U and Th, the cosmogenic produced unstable isotopes within the detector components, neutrons, ^{222}Rn and ^{40}K. All these influences should be reduced by building the experiments deeply underground, using the pure materials for the detector components, minimizing their exposure to the cosmic rays and shielding them by low-active materials with high Z (e.g. Pb, Cu). Rn and its daughters can be well-suppressed by working in a pure nitrogen (air-free) atmosphere or placing the detector into the air-tight box. The principle of some experiments will be shortly described further.

Generally, the experiments detecting electrons can be divided into two groups - active and passive [6]. The former use the same material (^{76}Ge) as source and simultaneously as detector; that is their advantage. On the other hand they only can measure the sum energy of both electrons. The latter use different materials but they can provide more information like measurement of the energy and tracks of electrons, separately.

Semiconductor experiments are of the active type, where both the source and the detector are made of ^{76}Ge. They provide an excellent energy resolution ($\approx$ 5 keV at 2 MeV) but still they only measure the sum energy of two electrons. Their improvement is based on using the enriched High-Purity Germanium[1] (HPGe) detectors, on the background reduction and on the improvement of the analysis systems to distinguish between the single-site ($\beta\beta$-decay) and the multi-site (multiple Compton scattering) events.

Scintillator experiments are based on using scintillators made of $\beta\beta$-decay isotopes: e.g. ^{48}Ca in the form of CaF_2, or ^{116}Cd in the form of $CdWO_4$. They can be cheaply produced in larger amount (in comparison with ^{76}Ge), but the energy resolution is poor (10 % at 661 keV).

Cryogenic experiments use bolometers[2] working at a very low temperature of several mK. Studies using ^{130}Te in the form of TeO_2 crystals have been performed (see Appendix 1).

Ionisation experiments are of the passive type, where the emitters are in the form of gas (^{136}Xe) filling the detection chamber or in the form of thin foils (^{82}Se, ^{96}Zr, ^{100}Mo, ^{116}Cd, ^{150}Nd) of the different configuration (cylindrical, planar). They allow energy measurements and tracking of two electrons. The disadvantages are the energy resolution and the limited amount of source.

Geochemical experiments investigate the very old ores, which accumulated a significant amount of the daughter nuclei. The advantage of these experiments is the long exposure time of up to 10^9 years. But thanks to the problems with the determination of the accurate age of ore, excluding the other processes producing the daughters, avoiding a high initial concentration of the daughters and having the significant source strength, only ^{82}Se and ^{130}Te are usable. The detection is based on the isotopical anomalies due to $\beta\beta$-decay ($^{82}\text{Se} \rightarrow {}^{82}\text{Kr}$, $^{128,130}\text{Te} \rightarrow {}^{128,130}\text{Xe}$), which are measured by mass spectrometry.

Radiochemical experiments take advantage of the radioactive decay of daughter nuclei needing a shorter measuring time. They concentrate on the decays $^{232}\text{Th} \rightarrow {}^{232}\text{U}$ and $^{238}\text{U} \rightarrow {}^{238}\text{Pu}$ with characteristic Q-values of 0.85 MeV and 1.15 MeV, respectively.

[1] Ge should be produced in purity of less than one atom of impurity per 10^{12} atoms of Ge [17].

[2] bolometer = apparatus for the radiant heat measurement

Generally, the geochemical and the radiochemical experiments, as a consequence of their principle, provide less information about $\beta\beta$-decay, including the limited sensitivity in comparison with the other types of experiments mentioned.

At present and in the near future, there will be about 15 experiments measuring $\beta\beta$-decays (see Appendix 1). The latest results are listed in Tables 2.1 and 2.2. In the next section, two experiments - NEMO and Heidelberg-Moscow - will be shortly described.

2.1.2 NEMO experiment

The NEMO experiment [18] was designed to study the $0\nu\beta\beta$-decay for several isotopes (e.g. ^{100}Mo, ^{82}Se). The sensitivity of the detector for ^{100}Mo achieves the limit of about 10^{25} yr. The corresponding sensitivity for the effective neutrino mass $\langle m_\nu \rangle$ is of about (0.1 - 0.3) eV. The NEMO experiment is located at the Fréjus Underground Laboratory (Modane, France), 4,800 m.w.e. (m.w.e. = metre water equivalent).

NEMO 1.

NEMO 1 (see Figure 2.2) was the first version of this experiment. It had a very simple structure. It consisted of 64 Geiger cells mounted inside a copper box ordered in 8 parallel planes of 8 cells for the 3D event reconstruction.

Its aim was to measure and to understand the background in the laboratory and to prove the feasibility of such project. NEMO 1 took data during 18 months in various running conditions. It found out that the background in $E \lesssim 2$ MeV originates from the natural radioactivity γ-flux, in the region of energies 3 MeV $< E <$ 8 MeV, the main contribution came from neutrons, and for $E >$ 8 MeV the remaining muon flux was identified.

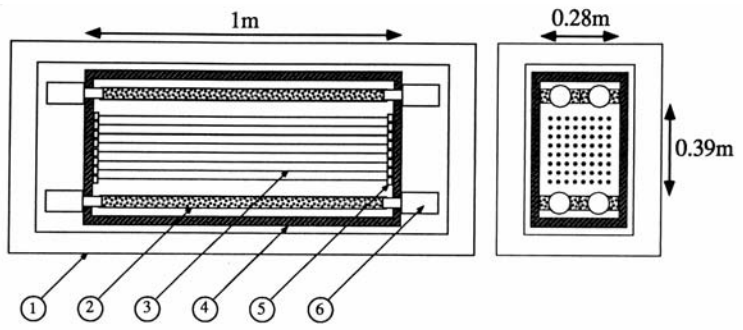

Figure 2.2: The NEMO 1 prototype: (1) Shielding, (2) Plastic scintillators, (3) Wires of Geiger cells, (4) Copper wall (1 cm thick), (5) Cathode ring, (6) Phototube, ref. [18].

NEMO 2.

NEMO 2 (see Figure 2.3) consisted of 1 m^3 tracking volume filled with helium gas and 4 % admixture of ethylalcohol at the atmospheric pressure. The tracking part was created by the octagonal cells (32 mm in diameter, 1 m in length), each with a central nickel wire (100 μm in diameter) surrounded by the 8 ground wires. On both cell ends, there was a copper ring (29 mm in diameter) used as a pick up electrode. Thanks to the filling gas properties, electrons with energy down to 100 keV could be detected. The wire cells worked in the Geiger mode with a voltage of 1.9 kV on the anode. The detector consisted of vertical

planes, where the central one contained a source foil (1×1 m^2). On each side of the source foil, there were 10 planes of 32 cells each, allowing a 3D orientation and event reconstruction, as well. Both vertical sides were covered by a calorimeter made of scintillators, where two different configurations were used (2 planes of 64 scintillators (12×12×2.25 cm^3) associated with standard photomultiplier tubes (PMT's) - ^{100}Mo measurement; 2 planes of 25 scintillators (19×19×10 cm^3) with the low radioactive glass PMT's). In addition, tracking volume and scintillators were covered with 5 cm of Pb and 20 cm of Fe.

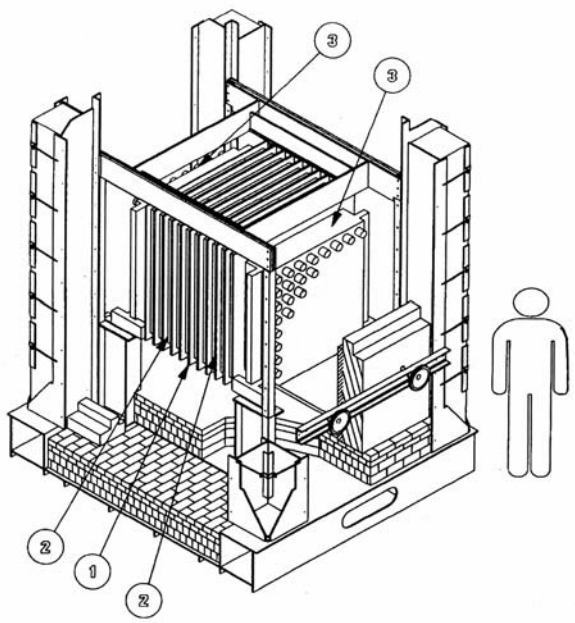

Figure 2.3: The NEMO 2 prototype: (1) Central frame with metallic foil, (2) Tracking device of 10 frames with 2×32 Geiger cells each, (3) Scintillator walls of 8×8 counters. The shielding is not shown, ref. [18].

NEMO 2 took measurement in 2e, $e\gamma$, $e\gamma\alpha$ modes. It observed no 2e event below 2.2 MeV coming from very pure Cu-foil used, and a clear signal of a thousand of $2\nu\beta\beta$ events emanating from pure enriched Mo-foil with no event below 2.5 MeV. The search for one-electron events allowed to put some limits for the β-emitter nuclide contamination. Events caused by neutrons (e^+e^- pairs produced in source foil, $E \gtrsim 3$ MeV) were eliminated by magnetic field. The Rn presence inside of NEMO 2 detector was proved. It implied the additional isolation of the further detectors. The measured results are in Table 2.3.

Isotope	$T_{1/2}^{2\nu\beta\beta}$ (yr)	$T_{1/2}^{0\nu\beta\beta}$ (yr)	$T_{1/2}^{0\nu(2)\chi\beta\beta}$ (yr)
^{82}Se	$8.30 \pm 1.00 \pm 0.70 \times 10^{19}$	$> 9.5 \times 10^{21}$	$> 2.4 \times 10^{21}$
^{96}Zr	$2.10^{+0.8}_{-0.4} \pm 0.20 \times 10^{19}$	$> 1.0 \times 10^{21}$	$> 3.9 \times 10^{20}$
^{100}Mo	$9.50 \pm 0.40 \pm 0.90 \times 10^{18}$	$> 6.4 \times 10^{21}$	$> 5.0 \times 10^{20}$
^{116}Cd	$3.75 \pm 0.35 \pm 0.21 \times 10^{19}$	$> 5.0 \times 10^{21}$	$> 1.2 \times 10^{21}$

Table 2.3: The results from NEMO 2, ref. [15].

NEMO 3.

NEMO 3 is the latest version of the experiment constructed on the basis of the results of its predecessors [18, 19]. Its structure allows the measurement of more event parameters: the full energy released, such as the single electron energy, the angle between emitted electrons, the coordinates of events, and so on. It uses several $\beta\beta$-sources arranged into 20 sectors, as shown in Figure 2.4. The sensitivity of measurement after 5 years will achieve $\approx 10^{25}$ yr for $0\nu\beta\beta$-decay ($\langle m_\nu \rangle \approx (0.1 - 0.3)$ eV), $\approx 10^{23}$ yr for $0\nu(2)\chi\beta\beta$-decay and $\approx 10^{22}$ yr for $2\nu\beta\beta$-decay.

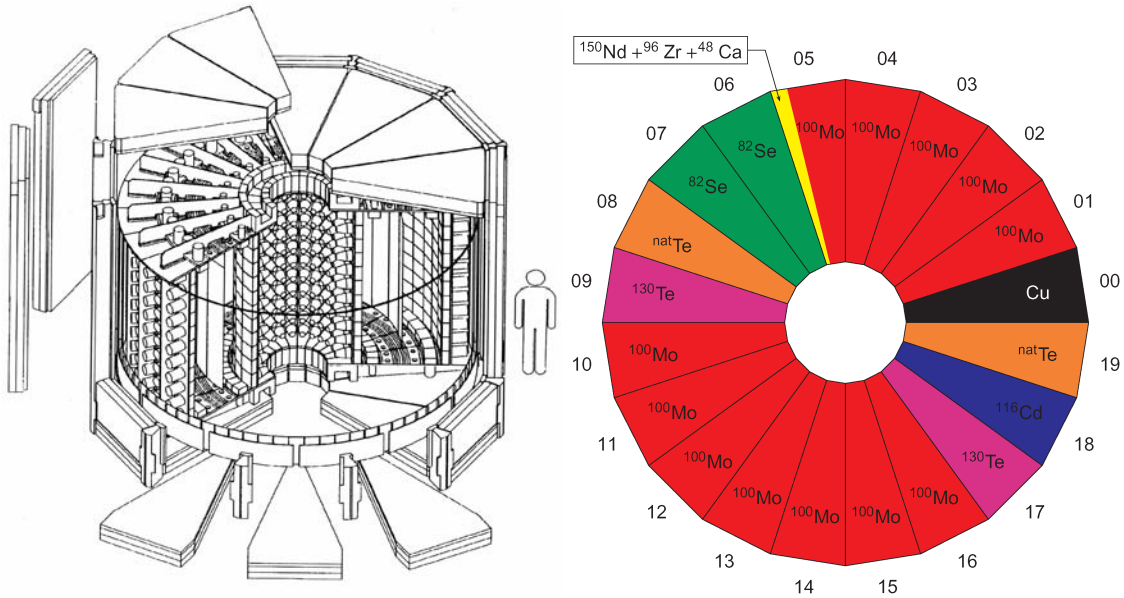

Figure 2.4: Left: The NEMO 3 prototype scheme. Right: The NEMO 3 source arrangement, ref. [18, 19].

The detector has a regular icosahedron shape (4 m in diameter, 3 m in height). The tracking volume is filled with helium with admixture of ethylalcohol (all 7 mbar (= 7 hPa) above atmospheric pressure) and is vertically divided by a thin source foil (≈ 50 μm) into an inner and an outer concentric cylinders with walls covered by the calorimeters made of plastic scintillators. The whole system uses 6,180 Geiger cells (2.7 m in length) parallel to the vertical axis of the detector. The energy and the time-of-flight are measured by plastic scintillators covering the two concentric surfaces, which are constructed of 1,940 low radioactive PMT's of two different types (3" and 5"). As well, the magnetic field of 25 Gauss (2.5×10^{-3} Tesla) is used to eliminate the background contribution of pair creation and electrons incoming from outside and crossing the detector. The shielding is provided by Pb, Fe, wood, polyethylene and water, thus, the background is efficiently suppressed. Monte Carlo simulations show that on this level the main source of background is radon. Finally, the measured nuclides are: ^{100}Mo (6.9 kg), ^{82}Se (0.93 kg), ^{116}Cd (0.4 kg), ^{130}Te (0.45 kg), ^{150}Nd (36.5 g), ^{96}Zr (9.43 g) and ^{48}Ca (6.99 g); the other isotopes (Cu, natural Te) serve as background estimation [19].

NEMO 3 takes data since 14 February 2003 [20]. The first results published in May 2003 (1,200 hours of the operation in total) are listed in the Table 2.4.

After NEMO 3, approximately in year 2007, the next version is planned to be built [11]. Its principle will be the same as in the previous versions with planar geometry (4 modules). It will probably contain about 100 kg of ^{82}Se (or other nuclei) allowing

Isotope	$T_{1/2}^{2\nu\beta\beta}$ (yr)	$T_{1/2}^{0\nu\beta\beta}$ (yr)
^{82}Se	$9.10 \pm 0.40 \pm 0.90 \times 10^{19}$	$> 4.0 \times 10^{22}$ (90 % CL)
^{100}Mo	$7.40 \pm 0.05 \pm 0.80 \times 10^{18}$	$> 1.0 \times 10^{23}$ (90 % CL)
^{116}Cd	$3.90 \pm 0.30 \pm 0.40 \times 10^{19}$	$> 1.0 \times 10^{22}$ (90 % CL)
^{150}Nd	$7.00 \pm 0.70 \pm 0.70 \times 10^{18}$	$> 7.7 \times 10^{20}$ (90 % CL)

Table 2.4: The latest results from NEMO 3, ref. [20].

the sensitivity for $0\nu\beta\beta$-decay of about 10^{26} years ($\langle m_\nu \rangle \approx 0.05 - 0.11$ eV) in five years of operation. It is projected to use about 50 tons of plastic scintillators, about 5,000 low-background PMT's and roughly 30,000 Geiger cells. As shielding, 20 cm of Fe and 20 cm of borated polyethylene will be used.

	NEMO 2	NEMO 3
Energy threshold for scintillators	50 keV	30 keV
Energy resolution (FWHM) at 1 MeV	18 %	11-15 %
Time resolution at 1 MeV	275 ps	250 ps

Table 2.5: The comparison of NEMO 2 and NEMO 3 experimental characteristics, ref. [11, 18].

2.1.3 Heidelberg-Moscow experiment

Since 1995, the Heidelberg-Moscow experiment is located in the Gran Sasso Underground Laboratory (Italy) at a depth of 3,500 m.w.e. It operates with five p-type HPGe detectors of total active mass of 10.96 kg of 86 % enriched ^{76}Ge, corresponding to 125.5 mol of germanium [12]. Four of these detectors are placed in a common 30 cm thick lead shielding in a radon-free nitrogen atmosphere, surrounded by the neutron shielding (steel box centered inside a 10 cm boron-loaded polyethylene). Since August 1996 two layers of 1 cm thick plastic scintillator (1.8×1.8 m^2) on top of the setup are used as the muon anticoincidence shielding. The fifth detector is placed in a box with the inner 27.5 cm electrolytic copper and the 20 cm outer lead, and the boron-loaded polyethylene shielding below the steel box; this detector is not shielded against muons. It is also operated in a radon-free atmosphere. The parameters of the detectors are following: energy resolution in the range of 3.0-3.7 keV at 2.615 MeV, energy threshold is about 70 keV (with exception of the fifth detector used for the dark matter measurements, additionally).

The latest Heidelberg-Moscow experimental results are [12, 13, 14]:

$$
\begin{aligned}
T_{1/2}^{2\nu\beta\beta} &= (1.55 \pm 0.01^{+0.19}_{-0.15}) \times 10^{21} \text{ y}, \\
T_{1/2}^{0\nu\chi\beta\beta} &> 6.40 \times 10^{22} \text{ y (90 \% CL)}, \\
T_{1/2}^{0\nu\beta\beta} &= (0.8 - 18.3) \times 10^{25} \text{ y}, \langle m \rangle = (0.11 - 0.56) \text{ eV (95 \% CL)}.
\end{aligned}
$$

Chapter 3

Neutrino oscillations

The neutrino oscillations are the quantum mechanical processes representing a very important quality of neutrinos, allowing to measure neutrino masses as small as 10^{-5} eV or smaller, which are far beyond the direct kinematic tests [2]. The idea was for the first time presented by Bruno Pontecorvo in 1957 [21, 22]. The existence of three neutrino flavors being proved [1], only the formalism for three generation mixing will be briefly described.

As the neutrinos originate from the charged-current weak interaction, the weak-eigenstates ν_e, ν_μ and ν_τ exist. Each of them is created as a certain combination of the basic mass-eigenstates ν_1, ν_2 and ν_3 [2, 4, 5, 6]. These eigenstates are related via unitary matrix $\boldsymbol{U}$, which is not generally diagonal:

$$\nu_l = \sum_{i=1}^{3} \boldsymbol{U}_{li}\, \nu_i,\ \boldsymbol{U} = \begin{pmatrix} U_{e1} & U_{e2} & U_{e3} \\ U_{\mu 1} & U_{\mu 2} & U_{\mu 3} \\ U_{\tau 1} & U_{\tau 2} & U_{\tau 3} \end{pmatrix}, \tag{3.1}$$

where $l = e, \mu, \tau$. This mixing matrix, so-called MNS-matrix[1], similar to the quark CKM-matrix[2], depends on the three mixing angles $\theta_{12}, \theta_{13}, \theta_{23}$ and on the one δ or three $\delta_{12}, \delta_{13}, \delta_{23}$ CP-violating phases[3] in Dirac or Majorana case, respectively. In Dirac case it is expressed as [6]:

$$\boldsymbol{U_D} = \begin{pmatrix} c_{12}c_{13} & s_{12}c_{13} & s_{13}e^{-i\delta} \\ -s_{12}c_{23} - c_{12}s_{23}s_{13}e^{i\delta} & c_{12}c_{23} - s_{12}s_{23}s_{13}e^{i\delta} & s_{23}c_{13} \\ s_{12}s_{23} - c_{12}c_{23}s_{13}e^{i\delta} & -c_{12}s_{23} - s_{12}c_{23}s_{13}e^{i\delta} & c_{23}c_{13} \end{pmatrix}, \tag{3.2}$$

and for Majorana neutrinos as [6]:

$$\boldsymbol{U_M} = \begin{pmatrix} c_{12}c_{13} & s_{12}c_{13}e^{-i\delta_{12}} & s_{13}e^{-i\delta_{13}} \\ -s_{12}c_{23}e^{i\delta_{12}} - c_{12}s_{23}s_{13}e^{i(\delta_{13}+\delta_{23})} & c_{12}c_{23} - s_{12}s_{23}s_{13}e^{i(\delta_{13}+\delta_{23}-\delta_{12})} & s_{23}c_{13}e^{i\delta_{23}} \\ (s_{12}s_{23} - c_{12}c_{23}s_{13})e^{i(\delta_{13}+\delta_{23})} & -c_{12}s_{23}e^{i\delta_{23}} - s_{12}c_{23}s_{13}e^{i(\delta_{13}-\delta_{12})} & c_{23}c_{13} \end{pmatrix}, \tag{3.3}$$

where $s_{ij} = \sin\theta_{ij}$ and $c_{ij} = \cos\theta_{ij}$.

The system of eigenstates evolutes in time. If in time $t = 0$ the initial state is described by $|\nu(0)\rangle = |\nu_a\rangle = \boldsymbol{U}^*_{aj}|\nu_j\rangle$, at a later time t the state is $|\nu(t)\rangle = \boldsymbol{U}^*_{aj}e^{-iE_jt}|\nu_j\rangle$. Thus, the probability that the neutrino of a flavor eigenstate $|\nu_a\rangle$ is transformed into another one $|\nu_b\rangle$ is given by:

$$P(\nu_a \to \nu_b; t) = |\langle\nu_b|\nu(t)\rangle|^2 = |\boldsymbol{U}_{bj}e^{-iE_jt}\boldsymbol{U}^*_{aj}|^2. \tag{3.4}$$

[1] MNS-matrix = (Pontecorvo-)Maki-Nakagawa-Sakata matrix
[2] CKM-matrix = Cabibbo-Kobayashi-Masakawa matrix
[3] weak interaction breaks the parity conservation; C. S. Wu *et. al.*, 1957

In practice, several limiting cases are taken into account [2]. For a rest of this chapter, if L is the distance travelled by neutrino, the distance L depending probability will be used instead of the time t depending probability.

One will assume that the neutrino mass squared differences $\Delta m^2_{ij} = |m^2_i - m^2_j|$ have a hierarchy

$$|\Delta m^2_{21}| \ll |\Delta m^2_{31}| \simeq |\Delta m^2_{32}|.$$

This means that $m_1 \ll (\lesssim) m_2 \ll m_3$ (direct hierarchy) or $m_3 \ll m_1 \approx m_2$ (inverted hierarchy). This case is relevant for the atmospheric, reactor and accelerator neutrino experiments. In addition, consider $\Delta m^2_{21} L/(2E) \ll 1$ or even more $\Delta m^2_{21} \to 0$. Then the respective probabilities are:

$$P(\nu_e \to \nu_\mu; L) = 4|U_{e3}|^2|U_{\mu 3}|^2 \sin^2 \Delta_{31} = s^2_{23} \sin^2 2\theta_{13} \sin^2 \Delta_{31}, \tag{3.5}$$

$$P(\nu_e \to \nu_\tau; L) = 4|U_{e3}|^2|U_{\tau 3}|^2 \sin^2 \Delta_{31} = c^2_{23} \sin^2 2\theta_{13} \sin^2 \Delta_{31}, \tag{3.6}$$

$$P(\nu_\mu \to \nu_\tau; L) = 4|U_{\mu 3}|^2|U_{\tau 3}|^2 \sin^2 \Delta_{31} = c^4_{13} \sin^2 2\theta_{23} \sin^2 \Delta_{31}, \tag{3.7}$$

with $P(\nu_b \to \nu_a; L) = P(\nu_a \to \nu_b; L)$, where $\Delta_{ij} = \Delta m^2_{ij} L/(4E)$. Here the probabilities only depend on the third $\boldsymbol{U}$-column and on Δm^2_{31}.

Another limiting case is relevant for the solar neutrino experiments and for the very long baseline reactor oscillation experiments. Let us assume that $\Delta_{31} \simeq \Delta_{32} \gg 1$. Then the oscillations due to the Δm^2_{31} and Δm^2_{32} are very fast and lead to an average effect with the same probability for each transition (in vacuum):

$$P = 1 - \sin^2 2\theta_{12} \sin^2 \Delta_{21}. \tag{3.8}$$

Finally, consider that $U_{23} = 0$ with no requirement for mass squared differences. Then the probabilities are:

$$P(\nu_e \to \nu_\mu; L) = c^2_{23} \sin^2 2\theta_{12} \sin^2 \Delta_{21}, \tag{3.9}$$

$$P(\nu_e \to \nu_\tau; L) = s^2_{23} \sin^2 2\theta_{12} \sin^2 \Delta_{21}, \tag{3.10}$$

$$P(\nu_\mu \to \nu_\tau; L) = \sin^2 2\theta_{23}(-s^2_{12} c^2_{12} \sin^2 \Delta_{21} + s^2_{12} \sin^2 \Delta_{31} + c^2_{12} \sin^2 \Delta_{32}). \tag{3.11}$$

Oscillations in matter (MSW-effect; see Appendix 2, page 48) are more complicated [2]. Generally, the matter effects on $\nu_\mu \leftrightarrow \nu_\tau$ are much smaller than in cases with ν_e. In fact, the manifestation of the matter effects on neutrino oscillations is the resonance enhancement of the oscillation probability. In vacuum, the oscillation probability cannot exceed $\sin^2 2\theta_0$, and for small mixing angles it is always small. Matter can enhance neutrino mixing, and the probability of neutrino oscillations in matter can be large even if the mixing angle in vacuum is very small. Matter enhancing neutrino oscillations provides one of the several ways how to solve the solar neutrino problem (see section 5.3); matter effects on oscillations of solar and atmospheric neutrinos, in supernovae and in the early universe may also be strongly affected by matter.

3.1 Neutrino oscillation experiments

There are two types of neutrino oscillation experiments, appearance and disappearance searches [5]. Appearance experiments look for the anomalous appearance of ν_e or ν_τ events in a relatively pure ν_μ beam and they are mainly sensitive to uncertainties in background sources of appearance neutrinos. The disappearance experiments search for the changes

in the neutrino flux of accurately known composition. All these deviations are studied as the functions of the distance L travelled by neutrinos and the neutrino energy E.

The experimental results are typically displayed on a two dimensional plot of Δm^2 versus $\sin^2 2\theta$ assuming an effective two component mixing formula. The $\sin^2 2\theta$ parameter sets the size of oscillation effects and thus the needed statistical sample. The Δm^2 value sets the distance to energy ratio needed for neutrinos to oscillate with an oscillation length given by $L_{osc} = \pi E/(1.27\Delta m^2)$.

The oscillation plot shows two main regions. If an oscillation signal is observed with a probability given by $P_{osc} = P_{signal} + \delta P_{signal}$, then, within some confidence level, a region in the (Δm^2, $\sin^2 2\theta$) plane is allowed. But if an experiment sees no signal and limits the probability of a specific oscillation channel to be $P_{osc} < P$ at 90 % CL, then an excluded region is displayed in the (Δm^2, $\sin^2 2\theta$) plane [5].

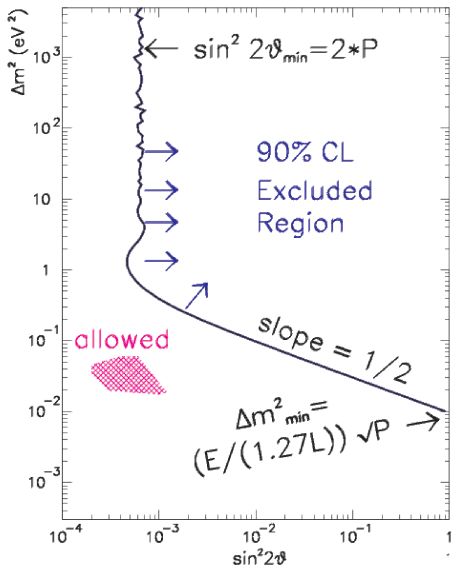

Figure 3.1: The oscillation plot, ref. [5].

3.2 Reactor experiments

3.2.1 Principle

The reactors are large sources of $\bar{\nu}_e$'s of the energy of several MeV, originating from the fission of the nuclear fuel (^{235,238}U, ^{239,241}Pu). The neutrino rates were measured for each isotope and are in very good agreement with the theoretical predictions [6]. The reactor experiments are of disappearance type, because the energies of the reactor $\bar{\nu}_e$'s ($\langle E \rangle \simeq 3$ MeV) are too small to allow the detection of $\bar{\nu}_\mu$'s and $\bar{\nu}_\tau$'s in charged current experiments [2]. To search for $\bar{\nu}_e \to \bar{\nu}_{\mu,\tau}$ oscillations, a positron spectrum is used [6]. It is measured at the several distances from the reactor or is calculated from the characteristics of the $\bar{\nu}_e$-flux produced by the reactor. The main reaction with the well-known cross section is:

$$\bar{\nu}_e + p \to e^+ + n, \tag{3.12}$$

while the threshold is of 1.804 MeV. The detection reaction is always the same, but the positron and the neutron detection strategies change. Normally, the coincidence tech-

niques are used between the annihilation photons and neutrons diffusing and thermalising within 10-100 μs. The major background contribution comes from the cosmic ray muons producing neutrons in the detector surrounding material [6].

3.2.2 Experimental status

Several experiments were done in the past (see Table 3.1), all using the fiducial mass less than 0.5 t with the distance reactor-detector shorter than 250 m. At present, the most important experiments are CHOOZ, Palo Verde and KamLAND [2, 4, 6].

Reactor	Power (MW)	Distance (m)
ILL-Grenoble (France)	57	8.75
Bugey (France)	2,800	13.6, 18.3
Rovno (USSR)	1,400	18.0, 25.0
Savannah River (USA)	2,300	18.5, 23.8
Gösgen (CH)	2,800	37.9, 45.9, 64.7
Krasnoyarsk (Russia)	?	57.0, 57.6, 231.4
Bugey III (France)	2,800	15.0, 40.0, 95.0

Table 3.1: The list of the terminated reactor experiments. The thermal power of reactors and the distance reactor-detector(s) are given, ref. [6].

The CHOOZ experiment (France) is located underground with a shielding of 300 m.w.e. and at the distance of about 1,030 m from two 4.2 GW reactors, thus it is sensitive to smaller Δm^2. The main target is a 4.8 t Gd-loaded scintillator, detecting annihilation photons in coincidence with neutron capture of Gd-producing gammas with a total energy up to 8 MeV.

The Palo Verde experiment (Phoenix, Arizona, USA) consists of 12 t liquid scintillator loaded with Gd, which is divided into 11×6 modules forming an array. A signal is registered, when three modules detect an event simultaneously. The shielding is of about 46 m.w.e. and the distance from three reactors with a total thermal power of 10.2 GW is about 750(820) m.

Both previous experiments found no indication of the disappearance of reactor $\bar{\nu}_e$'s. The measured ratios R of the observed and expected number of $\bar{\nu}_e$ events are [4]:

$$R_{CHOOZ} = 1.01 \pm 2.80\% \pm 2.70\%, \; R_{Palo\ Verde} = 1.01 \pm 2.40\% \pm 5.30\%.$$

Analysing the CHOOZ data, the best-fit oscillation parameters are [4]:

$$\Delta m^2_{CHOOZ} = 2.5 \times 10^{-3}\ \text{eV}^2, \;\; \sin^2 2\theta_{CHOOZ} \lesssim 1.5 \times 10^{-1}.$$

The KamLAND experiment (Japan) started in January 2002 detecting the $\bar{\nu}_e$-flux of many Japanese and Korean surrounding reactors (80% of the flux come from 26 reactors with the distance of 138-214 km). KamLAND consists of 1 kt liquid scintillator located at the depth of 1 km in Kamioka mine. It detects both annihilation photons and 2.2 MeV delayed photons from neutron capture. The ^{238}U and ^{232}Th Earth background is excluded by applying a cut of $E_{prompt} \gtrsim 2.6$ MeV.

During 145.1 days, 54 $\bar{\nu}_e$'s were observed. The expected event number in no oscillation case is $N_{expected} = 86.8 \pm 5.6$, the background event number $N_{background} = 0.95 \pm 0.99$ and the ratio is [4]:

$$R_{KamLAND} = \frac{N_{observed} - N_{background}}{N_{expected}} = 0.611 \pm 0.085 \pm 0.041.$$

In KamLAND the prompt energy spectrum was also measured. The prompt energy is connected with the $\bar{\nu}_e$-energy through the relation $E_{prompt} = E_{\bar{\nu}_e} - 0.8\ \text{MeV} - \overline{E_n}$, where $\overline{E_n}$ is the average neutron energy and $0.8\ \text{MeV} = m_n - m_p - m_e$. The KamLAND best-fit oscillation parameters are [4]:

$$\Delta m^2_{KamLAND} = 6.9 \times 10^{-5}\ \text{eV}^2,\ \sin^2 2\theta_{KamLAND} = 1.0.$$

Thus, KamLAND provided a strong evidence for neutrino oscillations obtained for the first time with the terrestrial reactor $\bar{\nu}$'s with the well-controled initial flux, meaning that SMA, LOW and VAC solar neutrino problem solutions are excluded and the best one remains the LMA (see section 5.3) taking into account the MSW effect (LMA-MSW) [4].

3.3 Accelerator experiments

3.3.1 Principle

The high energy accelerators are the second powerful terrestrial neutrino sources and the experiments using them are of both appearance and disappearance types [6]. The accelerators produce a high energy proton beam aimed at a fixed target. The produced secondary pions and kaons decay and create the neutrino beams mainly consisted of ν_μ's. A detection process is then based on the charged-current reaction:

$$\nu_l + N \rightarrow l + X, \tag{3.13}$$

where $l = e, \mu, \tau$. N is a nucleon and X a hadronic final state. That means, the oscillation detection requires the detectors registering all the neutrino flavors.

3.3.2 Experimental status

Accelerators at medium energy

These experiments observe neutrinos at medium energy ($E_\nu \approx$ 30-50 MeV). Several ones will be described at the following paragraphs.

KARMEN [6, 23] uses the neutrino beam from the neutron spallation source ISIS at Rutherford Appleton Laboratory (Chilton, UK), which is produced from a 800 MeV proton beam interacting with a massive target (Cu, Ta, or U). The well-known time structure of the ISIS proton pulses allows a clear separation of ν-induced events from background. The KARMEN detector is a rectangular high resolution liquid scintillation calorimeter located at a mean distance of 17.7 m from the ISIS target studying oscillations of $\bar{\nu}_\mu$'s. The results obtained from February 1997 to March 2001, are shown in Figure 3.2 (left).

The LSND is a 167 t of mineral oil based liquid scintillation detector using scintillation and Čerenkov light detection. The experiment is 30 m from LAMPF beam stop (Los Alamos, USA) under 12° with respect to the proton beam. It studies oscillations of ν_μ's and $\bar{\nu}_\mu$'s. Results from measurements during 1993 and 1998 are shown in Figure 3.2.

The best-fit oscillation parameters of both experiments are [23]:

$$\sin^2 2\theta_{\text{KARMEN}} = 1,\ \Delta m^2_{\text{KARMEN}} = 100\ \text{eV}^2,$$
$$\sin^2 2\theta_{\text{LSND}} = 3 \times 10^{-3},\ \Delta m^2_{\text{LSND}} = 1.2\ \text{eV}^2.$$

The LSND results are very controversial [5, 23, 26], because it detected $87.9 \pm 22.4 \pm 6.0$ events over expectation with an oscillation probability of $(0.264 \pm 0.067 \pm 0.045)$ % and

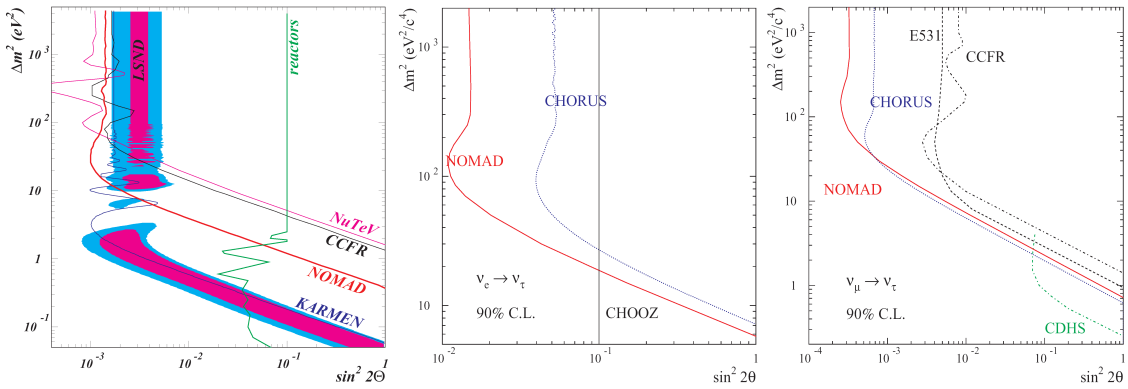

Figure 3.2: The 90 % CL exclusion region in the $\Delta m^2 - \sin^2 2\theta$ plane with the results of accelerator experiments (left). The current status of $\nu_e \rightarrow \nu_\tau$ (center) and $\nu_\mu \rightarrow \nu_\tau$ (right) oscillation searches obtained by CHORUS and NOMAD, ref. [24, 25].

obtained the Δm^2 parameter so large. The explication can be the existence of "sterile" neutrino(s). As the three different Δm^2 values exist ($\Delta m^2_{\text{sol}} = 5\times10^{-5}\text{eV}^2$, $\Delta m^2_{\text{atm}} = 2.5\times10^{-3}\text{eV}^2$ and $\Delta m^2_{\text{LSND}} = 1.2\text{eV}^2$), four mass-eigenstates are expected, thus, the mass hierarchies shown in the Figure 3.3 are possible. The theoretical apparatus for four-neutrino mixing is already developed, but many problems connected with sterile neutrinos exist; their observability via oscillations is difficult, because they cannot be affected by matter and at this moment, there exists no direct way for their detection.

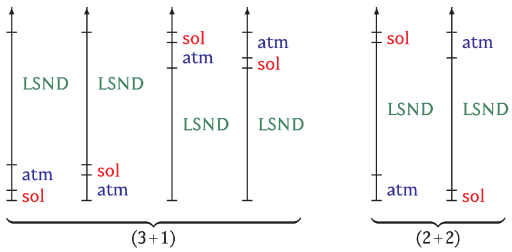

Figure 3.3: The six four-neutrino mass spectra, divided into the classes (3+1) and (2+2), ref. [26].

The MiniBooNE experiment (FermiLab) can confirm or exclude LSND's result [2, 27, 28]. It uses a 1 GeV neutrino beam produced at 8 GeV proton Booster. The detector is a sphere (12 m in diameter) filled with 950,000 liters of the pure mineral oil, surrounded by 1,280 PMT's. In addition, this detector allows the study of supernova and relic neutrinos and exotic particles. The data taking started in September 2002 and the first results will be available in 2005. An extension - the second detector - BooNE is under preparation.

Another experiments with medium energy neutrinos are prepared at CERN, where the PS neutrino beam with an average energy of 1.5 GeV will be received in locations 128 m and 850 m far.

Accelerators at high energy

The neutrinos used in these experiments have energies in the GeV-region [6]. Now, two CERN experiments will be described.

Both were designed to improve the existing limits on $\nu_\mu \rightarrow \nu_\tau$ oscillations by an

order of magnitude [24, 25]. They use a beam of 25 GeV neutrinos, produced at WANF (West Area Neutrino Facility) at CERN, when the beryllium beam dump is hit by 450 GeV protons. The beam is almost pure ν_μ with 6 % $\bar{\nu}_\mu$ and 1 % ν_e contamination. To suppress the uncertainties, the NA56 experiment measures the resulting pion and kaon spectra. The experiments are 823 m (CHORUS) and 835 m (NOMAD) far from the beam dump. Both experiments differ in their detection technique. CHORUS searches for tau lepton and its decay, whereas NOMAD relies on kinematic criteria.

The active target of CHORUS consists of a nuclear emulsion of 770 kg total mass with scintillator fibre tracker interleaved. Behind the target are placed a hexagonal spectrometer magnet for momentum measurement and a high resolution spaghetti calorimeter for measuring hadronic showers and a muon spectrometer. The emulsion scanning is performed with high-speed CCD microscopes.

NOMAD uses drift chamber (target) and tracking medium. In total, 44 chambers are located in the magnetic field of 0.4 Tesla. They are followed by a transition radiation detector for e/π separation and further electron identification devices in form of a preshower detector and an electromagnetic lead glass calorimeter. A hadronic calorimeter and a set of 10 drift chambers for muon identification follow. Another iron-scintillator calorimeter of about 20 t target mass is installed in front of the drift chambers.

The measured parameters - oscillation probabilities are [25]: $P(\nu_\mu \to \nu_\tau) < 3.4 \times 10^{-4}$ (CHORUS), $P(\nu_\mu \to \nu_\tau) < 1.68 \times 10^{-4}$ (NOMAD), $P(\nu_e \to \nu_\tau) < 2.6 \times 10^{-2}$ (CHORUS), $P(\nu_e \to \nu_\tau) < 1.68 \times 10^{-2}$ (NOMAD) all for 90 % CL. For $\nu_\mu \to \nu_e$ channel, the results are: $\Delta m^2 > 0.4$ eV^2 for maximal mixing, $\sin^2 2\theta < 1.2 \times 10^{-3}$ for larger Δm^2. Thus, NOMAD excludes the LSND evidence for $\Delta m^2 > 10$ eV^2 (see Figure 3.2 (left)).

3.3.3 New experiments

The future accelerator experiments [6] will focus on several topics: (1) the improvement of the oscillation parameters with the respect to CHORUS and NOMAD, (2) the check of the LSND evidence, and (3) the increase of the source-detector distance to probe smaller Δm^2 and direct comparability with the atmospheric scales.

Short and medium baseline experiments: One of these experiments, TOSCA, is prepared at CERN and it will combine the features from NOMAD and CHORUS [6].

Long baseline experiments: *K2K: KEK-Superkamiokande*: This experiment uses a 1 GeV neutrino beam (produced by 12 GeV protons) sending from KEK to Super-Kamiokande (235 km). The detection method is the same as in the case of atmospheric neutrinos (see section 4.1). The experiment is in the operation. One run started in January 2003 and another will start in 2004 with more energetic proton beam (50 GeV) [29]. *MINOS: Fermilab-Soudan*: The beam is produced at the Main Injector at Fermilab and is sent 735 km away to the Soudan mine. The detector is made of 8 kt magnetized Fe toroids in 600 layers with 2.54 cm thick, interrupted by about 20,000 m^2 active detector planes in form of plastic scintillator strips with x and y readout to obtain the necessary tracking information. *CERN-Gran Sasso*: This European experiment uses a neutrino beam produced at CERN, that is sent down to Gran Sasso Laboratory (732 km) .

The other experiments not mentioned, yet, planned to be located in one of the laboratories named above or in the other ones, are listed in Appendix 1.

Chapter 4

Atmospheric neutrinos

The atmospheric neutrinos ($\nu_e, \nu_\mu, \bar{\nu}_e, \bar{\nu}_\mu$) are the products of hadronic showers caused by the primary cosmic rays interacting within the atmosphere at the height of even 30 km. The main mechanism can be described as [2, 6]:

$$\begin{matrix}\text{cosmic ray}\\ \text{particles}\end{matrix} + \text{Air} \rightarrow K^{\pm}, K^0_L, K^0_S, \pi^{\pm}, \mu^{\pm}, \ldots \tag{4.1}$$

The neutrino flux depends on three main factors: the cosmic ray composition and spectrum, the geomagnetic cutoff, and the neutrino yield of the hadronic interactions in the atmosphere [2, 3, 4, 6]. The lower-energy neutrinos ($E \lesssim 1$ GeV) predominantly originate from π- and μ-decay ($\pi^{\pm} \rightarrow \mu^{\pm} + \nu_\mu(\bar{\nu}_\mu)$, $\mu^{\pm} \rightarrow e^{\pm} + \nu_e(\bar{\nu}_e) + \bar{\nu}_\mu(\nu_\mu)$) approximately leading to fluxes $\nu_\mu \sim \bar{\nu}_\mu \sim 2\nu_e$ or $\nu_e/\bar{\nu}_e \sim \mu^+/\mu^-$, whereas for energies above 1 GeV the ratio ν_e/ν_μ drops quickly. At further higher energies the main $\nu_{e,\mu}$-source is K^0_L-decay ($K^0_L\ (\equiv\ K^0_{e3}) \rightarrow \pi^{\pm} + e^{\mp} + \nu_e(\bar{\nu}_e)$, $K^0_L\ (\equiv\ K^0_{\mu 3}) \rightarrow \pi^{\pm} + \mu^{\mp} + \nu_\mu(\bar{\nu}_\mu)$), whereas the prompt neutrinos from the charm decays contribute only in the region above 10 TeV.

Neutrinos with energy in the interval 0.3 GeV $\lesssim E_\nu \lesssim$ 3.0 GeV come from reactions with particles in the energy range 5 GeV $\lesssim E_\nu \lesssim$ 50 GeV strongly affected by the geomagnetic cutoff depending on the gyroradius of the particles (introducing a factor A/Z between nuclei and protons of the same energy). Besides, the neutrino production depends on the energy per nucleon E/N. As well, particles with energy $\lesssim$ 20 GeV are affected by the 11-year Sun activity cycle, preventing (in maximum) low-energy cosmic rays to penetrate the inner solar system. Neutrinos with energy below 1 GeV are detected via horizontal or upward-going ("up-going") muons produced in charged-current reactions, where the dominant part of muons originates from events corresponding to neutrino energy 10 GeV $< E_\nu <$ 10^4 GeV. For cosmic ray particles of energies higher than $10^5/N$ only contribution of about 15 % to up-going muon flux is registered [2, 6].

Several theoreticians dwelled on calculating the atmospheric neutrino flux considering different variants of influences, but their results differed by as much as 20-30 % [2]. Thus, the Monte Carlo (MC) simulation of the hadronic cascades in the atmosphere was created (including all the effects mentioned above, together with for example muon polarization) to calculate the neutrino spectra.

In practice, two ratios of ν_μ- and ν_e-fluxes (events) were investigated [6]: one, the measured (μ/e) ratio, and the other so-called "double ratio" $R(\mu/e)$ of experimental values versus Monte Carlo predictions:

$$(\mu/e) = \frac{\nu_\mu + \bar{\nu}_\mu}{\nu_e + \bar{\nu}_e}, \quad R(\mu/e) = \frac{(\mu/e)_{exp}}{(\mu/e)_{MC}}. \tag{4.2}$$

Whereas the (μ/e) ratio calculations predict its dependence on neutrino energy and on the zenith-angle (approaching 2 for low energies, but exceeding it for higher energy neutrinos with trajectories close to vertical), the double ratio $R(\mu/e)$ is still approximately 0.6. The calculations of R for E_ν in interval of 0.4-1.0 GeV agree within 5 %. This discrepancy between the registered and predicted atmospheric neutrino fluxes was called the atmospheric neutrino anomaly, whose existence was independently confirmed by experiments listed in Table 4.1.

Experiment	R
Super-Kamiokande (sub GeV)	$0.68 \pm 0.02 \pm 0.05$
Super-Kamiokande (multi GeV)	$0.68 \pm 0.04 \pm 0.08$
Soudan 2	$0.61 \pm 0.15 \pm 0.05$
IMB	$0.54 \pm 0.05 \pm 0.11$
Kamiokande (sub GeV)	$0.60^{+0.06}_{-0.05} \pm 0.05$
Kamiokande (multi GeV)	$0.57^{+0.08}_{-0.07} \pm 0.07$

Table 4.1: The compilation of the R ratio measurements. $R = 1$ corresponds to the no oscillation case, ref. [2, 6].

Another evident effects related to the atmospheric neutrinos are the up/down asymmetry and the zenith-angle dependent deficiency of the muon neutrino flux, which are interpreted as the proof of neutrino oscillations. These phenomena will be described in the next section devoted to the Super-Kamiokande experiment giving the most convincing evidence for them.

4.1 Super-Kamiokande experiment

Experiment description

Super-Kamiokande (SK) is a water Čerenkov detector in the form of a cylinder with a diameter of 39 m and height of 42 m with total contained mass of 50 kt (fiducial volume is about 22.5 kt) using about 13,000 PMT's [29]. The detector is installed about 1 km underground (2,700 m.w.e.) at the Kamioka zinc mine (200 km west of Tokyo).

The overburden sufficiently reduces the large surface flux of downward-going ("down-going") muons to a level easily discriminated by the data acquisition system. The detector is divided by an optical barrier into a cylindrical primary detector region (the "inner detector", ID) and a surrounding shell of water approximately 2.5 m thick (the "outer detector", OD) serving as a cosmic ray veto counter.

In the case of SK-I, the OD was instrumented with 1,885 20-cm diameter Hamamatsu PMT's, whereas the ID was originally lined with 11,146 inward-facing 50-cm PMT's providing 40 % photocathode coverage for detecting several-MeV solar neutrinos. In November 2001, about half of the 50-cm ID PMT's were destroyed in cascade of implosions.

The primary phase of the reconstruction lasted about 13 months and in December 2002, testing of new SK-II experiment began. Almost all 20-cm OD PMT's were rescued and as the sufficient spares were available, OD part was fully restored. The reconstruction of ID PMT's was divided into several steps, when the missing PMT's are added gradually. In December 2002, more than 50 % of all ID PMT's were redistributed regularly in the inner part, while the full performance will be reached in 2005; this upgraded experiment will be named SK-III. The ID PMT's are now contained in plastic housings with the acrylic domes over the photocathodes, while the bodies and bases of PMT's are enclosed in the PVC shells. Thus, the explosion possibility is minimalized, and if any happen, it cannot harm the other

PMT's. The advantage of the materials used is the minimal influence on the angular and energy resolution for atmospheric neutrinos and up-going muons, whereas the effective threshold for the solar neutrinos rose.

Experimental methods

The charged leptons originating in the CC neutrino interactions produce in ID the rings of Čerenkov light observed by the phototubes. The sharp rings are created by muon-like events, while the electrons produce the fuzzier ones. SK-Collaboration divided the atmospheric neutrino counts into several groups depending on the produced charged lepton energy. The fully contained (FC) events take place in the ID, where all the final state particles are detected, and no significant activity in OD is registered. The partially contained (PC) events originate, when the primary muons exit ID, thus OD registers appropriate energy. FC events are furthermore subdivided into sub-GeV (visible energy < 1.33 GeV) and multi-GeV (visible energy > 1.33 GeV) events. FC atmospheric neutrino events are observed at an average rate of about 8.2/day, while the PC event rate is about 0.6/day (total cosmic-ray muon rate at SK-II is 2.2/second) [29].

Muon neutrinos can also be detected indirectly via detecting the muons from ν_μ-interactions with detector surrounding material. To reduce the background from the atmospheric muons, only upward-going neutrino-induced muons are considered. These events are, as well, divided into two groups, the through-going muons (OD registers energy appropriate to exiting muon) with typical energy of 100 GeV and stopping muons (OD registers corresponding energy, but no particle exits) with average energy of about 10 GeV. The ID trigger works with almost 100 % efficiency for entering muons with momentum more than 200 MeV/c for all zenith-angles. Stopping muons, whose track length is larger than 7 m (~ 1.6 GeV) in ID are then selected for further analyses. Average up-going muon rate is about 1.4/day and about 0.3/day are the stopping tracks [29].

Zenith-angle distribution of the charged leptons measured experimentally disagree with those of their parent neutrinos. For multi-GeV neutrinos the average angle between the neutrino and charged lepton momentum is about 17°, while for sub-GeV neutrinos it is almost 60°. The distance L travelled by neutrinos before reaching the detector varies within a large range. For vertically (zenith angle $\theta_\nu = 0°$) down-going neutrinos $L \sim 15$ km, for horizontal trajectories ($\theta_\nu = 90°$) $L \sim 500$ km. The vertically up-going neutrinos ($\theta_\nu = 180°$) cross Earth along its diameter, thus, $L \sim 13,000$ km [29]. The zenith-angle distribution measured by SK is shown in Figure 4.1.

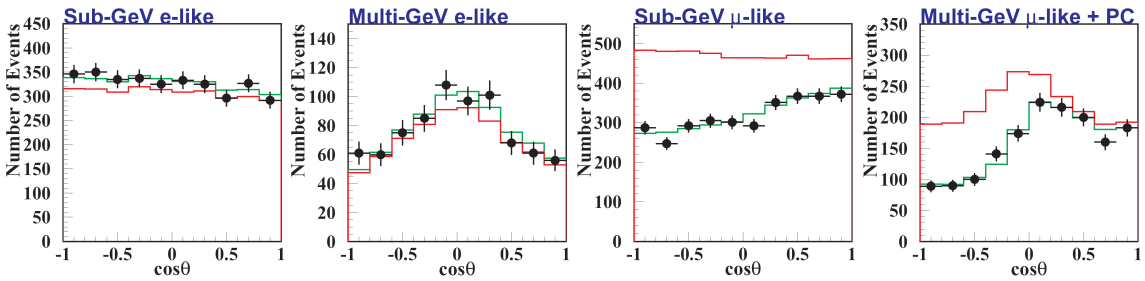

Figure 4.1: The atmospheric neutrino zenith-angle distribution. Points represent SK data, darker histogram corresponds to the expected no oscillation case, lighter one to the best-fit oscillation parameters, ref. [30].

It is evident, that zenith-angle distribution of e-like events agrees well with MC prediction, whereas μ-like events show zenith-angle dependent deficiency of the event number compared to the expectations, stronger for up-going neutrinos having the large

pathlengths. This pattern fits well with $\nu_\mu \to \nu_\tau$ or $\nu_\mu \to \nu_s$ oscillations. In multi-GeV μ-like region the pathlength decreases with increasing $\cos\theta$, thus, in this case of down-going ν_μ's ($\cos\theta > 0$) the oscillation length becomes larger than the pathlength and the oscillation effect disappears, while for up-going neutrinos the oscillation length is shorter than the pathlength and the oscillations become more significant. On the other hand, oscillation lengths for sub-GeV neutrinos are smaller, thus, although the down-going neutrinos have the shortest pathlengths, they are still larger than oscillation lengths, and the oscillations appear in the whole range of zenith angle. For $\nu_\mu \to \nu_\tau$ oscillations the measured data suggest [29]:

$$\Delta m^2_{SK-I} = (1.5 - 4.0) \times 10^{-3}\text{eV}^2, \ \sin^2 2\theta_{SK-I} = 1.0$$

with the best-fit parameters [4]:

$$\Delta m^2_{SK-I} = 2.5 \times 10^{-3}\text{eV}^2, \ \sin^2 2\theta_{SK-I} = 1.0.$$

Another parameter describing the deviations of the zenith-angle distribution is the up/down asymmetry A, where up means the event number, when $\cos\theta < 0.2$ and down the event number, when $\cos\theta > 0.2$. The values of A are expected to be about zero with minimal deviation coming from the geomagnetic effects taking into account. In addition, small positive asymmetry, thanks to the geographical location of SK, was predicted. Any significant deviation of A proves the neutrino oscillations or some other new phenomenon. In the case of μ-like multi-GeV events SK measured [2]:

$$A = \frac{U - D}{U + D} = -0.32 \pm 0.04 \pm 0.01, \tag{4.3}$$

while other cases are shown in Figure 4.2. For e-like events $A \simeq 0$ for all moments. At the μ-like case, asymmetry reaches zero only for low momenta because for these values the oscillation length is small and both oscillation contributions of up-going and down-going neutrinos are approximately the same. For the remaining cases, as the momentum increases, the ratio of oscillation length to up-going or down-going pathlength changes leading to, as mentioned above, different scenarios of oscillations.

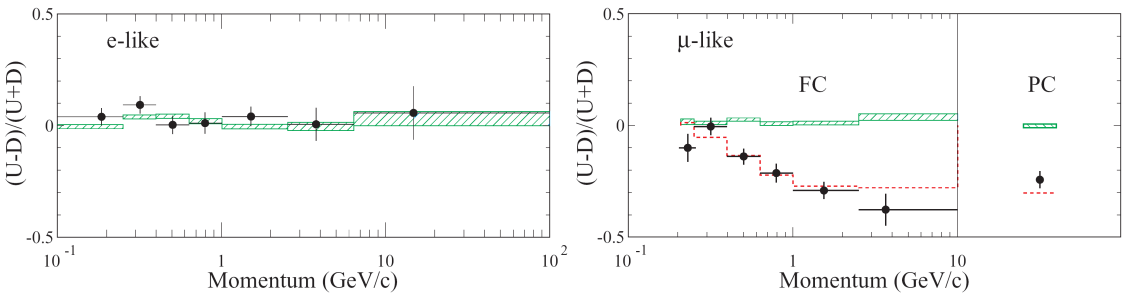

Figure 4.2: The up/down ratio for atmospheric neutrino events in SK and the integral representation of the angular distribution. Bars represent no-oscillation case, dashed histogram in right plot shows expectation for the best-fit oscillation parameters, ref. [29].

Chapter 5

Solar neutrinos

The Sun is our nearest source not only of energy, but of neutrinos, as well. The main process of the origin of stellar energy is a fusion of hydrogen into helium [31]:

$$4p + 2e^- \rightarrow {}^4\mathrm{He} + 2\nu_e + 26.73\mathrm{MeV} - E_\nu, \tag{5.1}$$

where E_ν is the energy taken away by the neutrinos. The whole reaction chain, including the fusion process (5.1), that is responsible for the majority of total energy, is the so-called *pp* cycle (see Figure 5.1); the carbon-nitrogen-oxygen (CNO) cycle (see Figure 5.2) produces less than 2 % of energy.

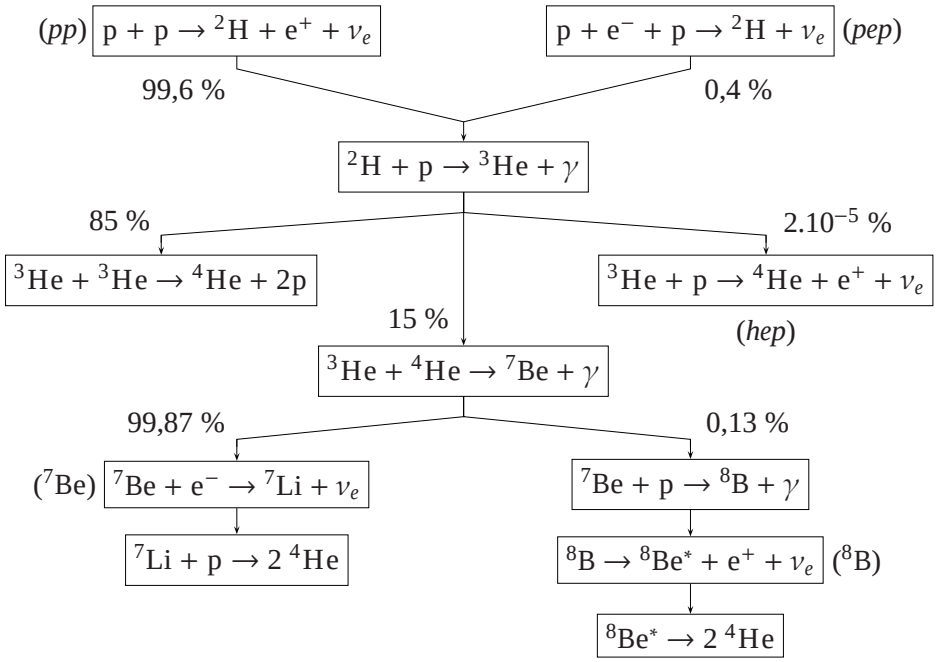

Figure 5.1: The *pp* cycle, ref. [2].

It is evident, that both cycles are, except the energy, the huge sources of neutrinos. Thanks to their properties (energy in the range 0.1 MeV $< E_\nu <$ 10 MeV, pathlength about 1.5×10^{11} m), these neutrinos are the unique tools to investigate the neutrino oscillations at very small Δm^2, smaller than 10^{-10} eV^2 [2, 31].

As well, the spectra of the main six neutrino-inducing reactions are well-known (see Figure 5.3). Three of those reactions - *pep* and the electron capture into two different ^{7}Be

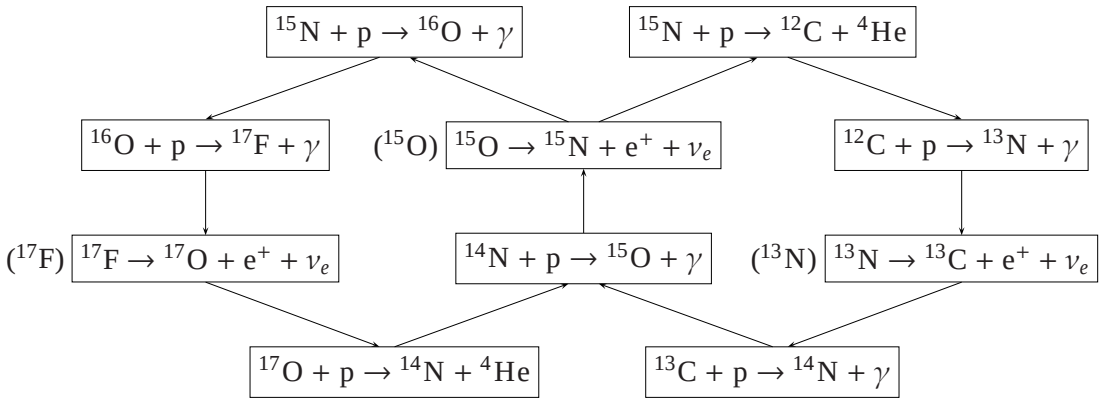

Figure 5.2: The CNO cycle, ref. [6].

final states - produce monochromatic ν_e lines, while the *pp*, *hep* and ^{8}B reactions have continuous energy spectrum [2].

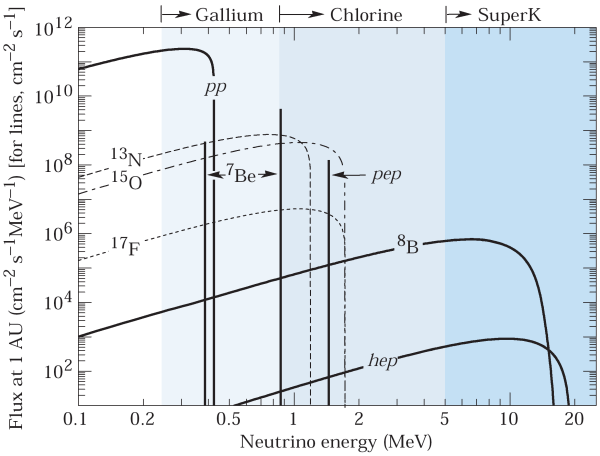

Figure 5.3: The solar neutrino spectra predicted by the standard solar model. The *pp* cycle spectra are marked by the solid curves, for CNO cycle the dotted curves are used, ref. [31].

5.1 Standard solar models

The fluxes of the solar ν_e's (see Table 5.1) are calculated with the help of the standard solar models (SSM) assuming the local hydrostatic equilibrium, thermonuclear nature of the solar energy, energy transfer by radiation and convection, and the requirements that the present values of the solar radius, mass, luminosity, and the He/H ratio can be reproduced as the result of the solar evolution [2, 5, 6, 31]. Nowadays, more than 20 different solar models exist, all based on the principles mentioned above. In addition, they take into account the many input parameters, such as the solar opacity, various nuclear cross sections, helium and heavy element diffusion, and so on. The accuracy of the input data is different, thus, the *pp* neutrino flux has an uncertainty about 1 %, ^{8}B neutrino flux about 20 %, while the *hep* flux (practically negligible) is known with the worst accuracy [2].

Reaction r	$\langle E\rangle_r$ (MeV)	E_r^{max} (MeV)	α_r (MeV)	ϕ_r (10^6 cm^{-2}s^{-1})	$\langle\sigma_{\rm Cl}\rangle_r$ (10^{-44} cm^2)	$R_{\rm Cl}^{(r)}$ (SNU)	$\langle\sigma_{\rm Ga}\rangle_r$ (10^{-44} cm^2)	$R_{\rm Ga}^{(r)}$ (SNU)
pp	0.2668	0.423 ± 0.003	13.0987	$59,500(1 \pm 0.01)$	-	-	0.117 ± 0.003	69.7
pep	1.445	1.445	11.9193	$140(1 \pm 0.015)$	0.16	0.22	$2.04^{+0.35}_{-0.14}$	2.8
hep	9.628	18.778	3.7370	0.0093	390	0.04	714^{+228}_{-114}	0.1
^{7}Be	0.3855, 0.8631	0.3855, 0.8631	12.6008	$4,770(1 \pm 0.10)$	0.024	1.15	$0.717^{+0.050}_{-0.021}$	34.2
^{8}B	6.735 ± 0.036	∼ 15	6.6305	$5.05(1^{+0.20}_{-0.16})$	114 ± 11	5.76	240^{+77}_{-36}	12.1
^{13}N	0.7063	1.1982 ± 0.0003	3.4577	$548(1^{+0.21}_{-0.17})$	0.017	0.09	$0.604^{+0.036}_{-0.018}$	3.4
^{15}O	0.9964	1.7317 ± 0.0005	21.5706	$480(1^{+0.25}_{-0.19})$	0.068 ± 0.001	0.33	$1.137^{+0.136}_{-0.057}$	5.5
^{17}F	0.9977	1.7364 ± 0.0003	2.363	$5.63(1 \pm 0.25)$	0.069	0.0	$1.139^{+0.137}_{-0.057}$	0.1
Total				65,400		$7.6^{+1.3}_{-1.1}$		128^{+9}_{-7}

Table 5.1: The characteristics of the neutrino-inducing reactions predicted by the BP2000 Standard Solar Model. The values listed for each reaction r: average ($\langle E\rangle_r$) and maximal (E_r^{max}) neutrino energy, average thermal energy release together with a neutrino from r (α_r), neutrino flux (ϕ_r), average neutrino cross section in Cl ($\langle\sigma_{\rm Cl}\rangle_r$) and in Ga ($\langle\sigma_{\rm Ga}\rangle_r$), the BP2000 neutrino capture rate prediction in Cl ($R_{\rm Cl}^{(r)}$) and in Ga ($R_{\rm Ga}^{(r)}$) measured in SNU's (1 SNU (Solar Neutrino Unit) = 10^{-36} captures per atom per second), ref. [32].

At present, the best solar models are BP2000 developed by Bahcall *et. al.* and the one developed by Turck-Chieze *et. al.* [31]. The former was constructed with the best available physics and input data, although no helioseismological constraints were used. In spite of that, for example, the calculated speed of sound as a function of the solar radius shows an excellent agreement with the helioseismologically determined speed of sound throughout the entire Sun. New version of BP2000 (so-called "BP2000 + New ^{8}B") is based on specifying one low-energy cross section factor for the ^{8}B reaction.

The latter is based on the standard theory of stellar evolution with the best available physics adopted, while some fundamental inputs such as the *pp* reaction rate and the heavy-element abundance in the Sun are seismically adjusted within the commonly estimated errors aiming at reducing the residual differences between the helioseismologically--determined and the model-calculated speed of sounds. Predicted values of the solar neutrino fluxes and event rates in Cl and in Ga using these models are listed in Table 5.1 and in Table 5.2.

5.2 Experimental status

Up to now, seven solar neutrino experiments published their results. Apparently, each experiment observed a deficiency in the event rate and neutrino flux. This phenomenon, known as the solar neutrino problem, will be explained in section 5.3.

5.2.1 Radiochemical experiments

The radiochemical experiments [2, 5, 31, 32] observe electron neutrinos via their absorption on the nuclei (^{37}Cl, ^{71}Ga) decaying through the orbital electron capture (originating Auger electrons are registered, too), giving no directional informations about the reactions:

$$^{37}\mathrm{Cl} + \nu_e \rightarrow {}^{37}\mathrm{Ar} + e^- \quad (\mathrm{E_{th}} = 814\ \mathrm{keV}), \tag{5.2}$$

$$^{71}\mathrm{Ga} + \nu_e \rightarrow {}^{71}\mathrm{Ge} + e^- \quad (\mathrm{E_{th}} = 233\ \mathrm{keV}). \tag{5.3}$$

After the detector exposure for a period of 2-3 half-lives of the product nuclei ($\tau_{1/2}^{Ar}$ = 34.8 days, $\tau_{1/2}^{Ge}$ = 11.43 days), the reaction products are chemically extracted and measured for a sufficiently long time by low-background proportional detector to

determine the exponentially decaying signal and the constant background. As predicted by SSM, the main contribution to the signal comes from ^{8}B neutrinos; ^{7}Be, *pep*, ^{15}O and ^{13}N contributions are significant, too (*pp* neutrinos can be registered only in Ga-experiments). Now, the description of solar neutrino experiments will be done, while the latest results are presented in Table 5.2.

Experiment	R(^{37}Cl $\rightarrow$ ^{37}Ar) (SNU)	R(^{71}Ga $\rightarrow$ ^{71}Ge) (SNU)	ϕ(^{8}B) (10^6 cm^{-2}s^{-1})
Homestake (1998)	$2.56 \pm 0.16 \pm 0.16$	-	-
GALLEX (1999)	-	$77.5 \pm 6.2^{+4.3}_{-4.7}$	-
GNO (2000)	-	$65.8^{+10.2+3.4}_{-9.6-3.6}$	-
SAGE (1999)	-	$67.2^{+7.2+3.5}_{-7.0-3.0}$	-
Kamiokande (1996)	-	-	$2.80 \pm 0.19 \pm 0.33$ (ES)
Super-Kamiokande (2001)	-	-	$2.348 \pm 0.025^{+0.071}_{-0.061}$ (ES)
SNO (2002)	-	-	$1.76^{+0.06}_{-0.02} \pm 0.09$ (CC)
	-	-	$2.39^{+0.24}_{-0.23} \pm 0.12$ (ES)
	-	-	$5.09^{+0.44+0.46}_{-0.43-0.43}$ (NC)
BP2000 *et. al.* (2001)	$7.6^{+1.3}_{-1.1}$	128^{+9}_{-7}	$5.05(1^{+0.20}_{-0.16}$
Turck-Chieze *et. al.* (2001)	7.44 ± 0.96	127.8 ± 8.6	4.95 ± 0.72
BP2000 + New ^{8}B	$8.59^{+1.1}_{-1.2}$	130^{+9}_{-7}	$5.93(1^{+0.14}_{-0.15}$

Table 5.2: The recent solar neutrino experimental results, ref. [31, 32].

Homestake

Homestake experiment located in Homestake Gold Mine (Lead, South Dacota, USA) in the depth of 1,478 m (4,200 m.w.e.) took data during 1970-1994 (108 runs) via reaction (5.2). It was a steel tank (6.1 m in diameter, 14.6 m long) containing about 615 t of tetrachloroethylen C_2Cl_4 (6×10^5 litres, 2.16×10^{30} Cl atoms), that measured ^{8}B, ^{7}Be, *pep* and *hep* neutrinos.

SAGE, GALLEX, GNO

The gallium experiments use reaction (5.3). They can measure *pp*, ^{7}Be, ^{8}B, *pep*, *hep*, ^{13}N, ^{15}O and ^{17}F. SAGE (Soviet-American Gallium Experiment) was installed in the Baksan Neutrino Observatory (northern Caucasus) 2,000 m (4,700 m.w.e.) deep. The detector was made of 50 t of metallic ^{71}Ga. Data were taken during 1990-2001 (92 runs). GALLEX (GALLium EXperiment) was located in the Gran Sasso Underground laboratory with 3,300 m.w.e. overhead shielding. 30.3 t of Ga in 101 t of gallium chloride solution ($GaCl_3$+HCl) was used as active material. Data were obtained from May 1991 to January 1997. From 1998, the GNO30 experiment of the newly defined Gallium Neutrino Observatory (GNO) became its successor, as well with 30.3 t of Ga, running between May 1998 and January 2000.

5.2.2 Kamiokande and Super-Kamiokande

Kamiokande and SK are both real-time Čerenkov experiments utilising the elastic scattering ($\nu + e^- \rightarrow \nu + e^-$) of neutrinos coming from ^{8}B and *hep* reactions [29]. That makes both experiments sensitive to all neutrino flavors, but the sensitivity to ν_e's is six times better than to ν_μ's and ν_τ's. Both can measure the directional correlation between the incoming neutrino and the recoil electron, helping to distinguish between solar neutrino signal and the background.

Kamiokande used, as a detector, 3,000 t of water surrounded with 948 PMT's. The energy threshold was E_{th}^{Kam} = 6.75 MeV. Data were collected from January 1987 to February 1995 (2,079 days in total). Thanks to the detector construction, Kamiokande measured for the first time the Sun-emitted neutrinos, observing the flux significantly less than predicted by SSM, the recoil electron spectrum was measured, as well, all in daytime and nighttime.

Super-Kamiokande is the successor of Kamiokande (Section 4.1). Solar neutrino data were obtained during 1996-2001 (1,496 days in total), when the SK-I was in the operation. The threshold energy was E_{th}^{SK} = 4.75 MeV. The average solar neutrino flux was smaller than, but consistent with, the Kamiokande-II result. The nighttime flux (N) is higher than the daytime one (D). SK measured the recoil electron spectrum, as well. Initially, its shape showed an excess at the high-energy end (> 13 MeV) in comparison with SSM expectations, but the reason was found to be the accumulation of statistics. Such as the up/down asymmetry, here the night/day asymmetry was measured [32]:

$$\mathcal{A}_{ND}^{SK} = \frac{N-D}{N+D} = 0.021 \pm 0.024. \tag{5.4}$$

The reason is that neutrinos detected during the night must travel longer distance through Earth than during the day, and the matter can affect more the original ν_e-flux. On contrary, a fraction of ν_μ's and ν_τ's produced as a result of the solar ν_e oscillations can be reconverted again into ν_e's.

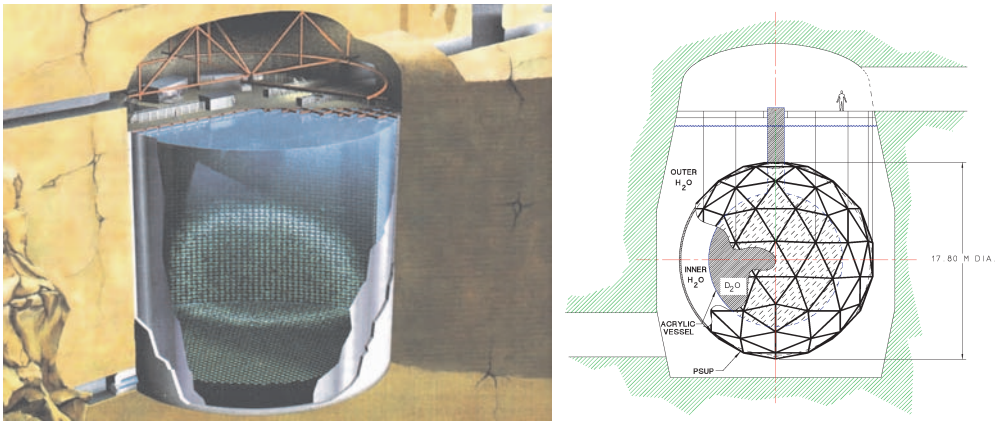

Figure 5.4: Super-Kamiokande (left) and Sudbury Neutrino Observatory (right) detectors, ref. [33, 34].

5.2.3 SNO

The detector consists of a transparent acrylic sphere 12 m in diameter, supported from a deck structure by ten synthetic fiber ropes (see Figure 5.4) [31, 32, 34]. The sphere holds 1,000 t of heavy water (D_20). Surrounding of the acrylic vessel is a geodesic structure 17.8 m in diameter made of stainless-steel struts and carrying 9,438 inward--looking PMT's. The barrel-shaped cavity, 22 m in diameter and 34 m in height, is filled with purified light water to provide support and shielding. SNO allows to measure ^{8}B solar neutrinos via charged-current (CC) reaction:

$$\nu_e + D \rightarrow e^- + p + p \quad (E_{th}^{SNO-CC} \simeq 8.2 \text{ MeV}), \tag{5.5}$$

neutral-current (NC) reaction:

$$\nu_l + D \rightarrow \nu_l + p + n \quad (E_{th}^{SNO-NC} \simeq 2.2 \text{ MeV}), \tag{5.6}$$

where $l = e, \mu, \tau$, and, finally, via elastic scattering (ES) reaction:

$$\nu_l + e^- \rightarrow \nu_l + e^- \quad (E_{th}^{SNO-ES} \simeq 7.0 \text{ MeV}). \tag{5.7}$$

The Q-value of the CC reaction is -1.4 MeV and the electron energy is strongly correlated with the neutrino energy, meaning that the CC reaction provides an accurate measurement of the ^{8}B solar neutrino spectrum shape. $\cos\theta_\odot$ is used for different distributions ($\theta_\odot$ is the angle with the respect to the direction from the Sun to Earth, see Figure 5.5) to distinguish between CC and ES reaction.

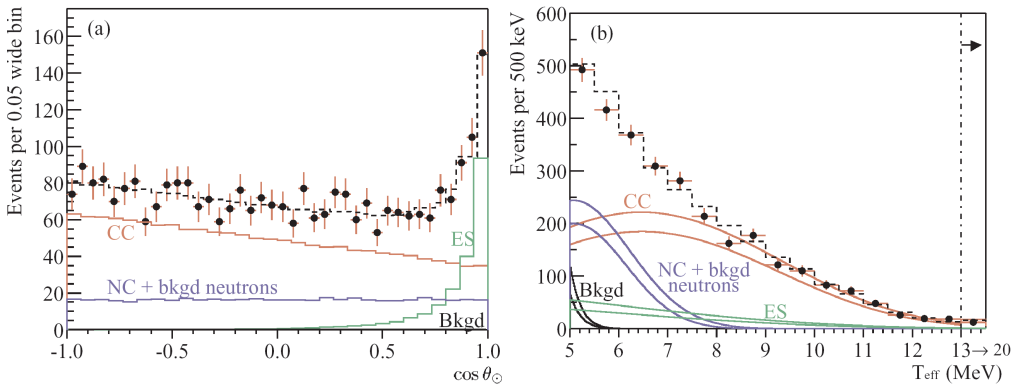

Figure 5.5: (a) The distribution of $\cos\theta_\odot$. (b) The kinetic energy spectrum with the Monte Carlo predicted CC, ES and NC + bkgd neutron events scaled to the fit results, and the calculated spectrum of Čerenkov background (Bkgd) events. The dashed lines represent the summed components, and the bands show $\pm 1\sigma$ uncertainties. All distributions are for $R \leq 5.5$ m, for events with $T_{eff} \geq 5$ MeV, ref. [35].

The energy threshold of the NC reaction is 2.2 MeV. In the pure D_2O, the NC reaction signal is neutron capture on deuterium producing a 6.25 MeV γ-ray. To enhance the low capture efficiency, 2.5 t of NaCl has been added into D_2O in the second phase of experiment. In the next phase, the discrete ^{3}He neutron counters are planned to be installed.

After the first publication of the results (^{8}B flux via CC, electron energy spectrum, $\cos\theta_\odot$ - consistent for no-oscillation case), in 2001, some problems with ^{8}B solar neutrino flux via ES occurred (very low statistics), new updated results were reported in April 2002 (306.4 days of measurement in total). Comparing the SNO CC results with SK EC ones, the evidence of a non-ν_e component in solar neutrino flux was obtained. The ^{8}B solar neutrino flux measurements via NC (consistent with SSM predictions) were reported, as well. The SNO night/day asymmetry (see Figure 5.6) value is [32, 36]:

$$\mathcal{A}_{ND}^{SNO} = 0.070 \pm 0.051. \tag{5.8}$$

5.3 Solution of the solar neutrino problem

All the experiments, which participated to the measurement of the solar neutrino characteristics, reported significantly less flux than expected by the SSM's. In an effort to solve this problem, many ways based on astrophysics measurements were developed. Unfortunately, all these solutions have very low probabilities and require non-trivial neutrino properties.

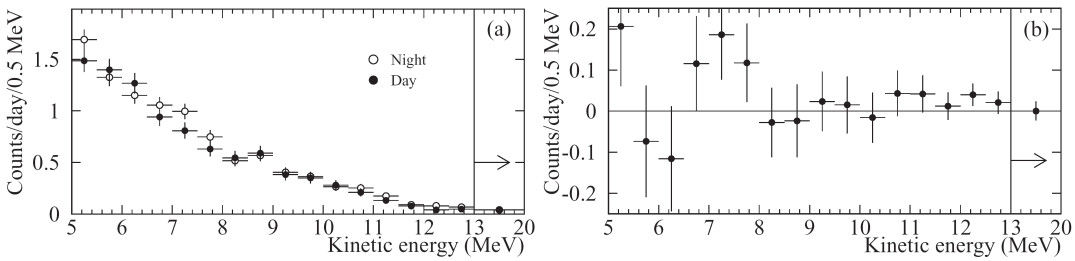

Figure 5.6: (a) The energy spectra for day and night (all signals and background contribute). (b) The night/day difference between the spectra (the day rate: 9.23 ± 0.27 events/day, the night rate: 9.46 ± 0.24 events/day), ref. [36].

The SNO and SK newest results showed another solution [4, 31, 32, 35, 36]. SNO and SK measured ν-fluxes via different reactions. Although SSM expected the equation $\phi^{CC}_{SNO}(\nu_e) = \phi^{ES}_{SK}(\nu_x)$, the SNO's first data indicated the discrepancy:

$$\phi^{ES}_{SK}(\nu_x) - \phi^{CC}_{SNO}(\nu_e) = (0.57 \pm 0.17) \times 10^6 \text{ cm}^{-2}\text{s}^{-1}. \tag{5.9}$$

This difference implied the direct evidence for existence of a non-ν_e active neutrino flavor component in the solar neutrino flux. The most plausible explanation was the ν_e oscillation.

From the measured $\phi^{CC}_{SNO}(\nu_e)$ and $\phi^{ES}_{SK}(\nu_x)$, the flux $\phi(\nu_{\mu \text{ or } \tau})$ and the total flux of the active ^{8}B solar neutrinos $\phi(\nu_x)$, can be deduced:

$$\phi(\nu_{\mu \text{ or } \tau}) = (3.69 \pm 1.13) \times 10^6 \text{ cm}^{-2}\text{s}^{-1}, \tag{5.10}$$

$$\phi(\nu_x) = (5.44 \pm 0.44) \times 10^6 \text{ cm}^{-2}\text{s}^{-1}. \tag{5.11}$$

Equation (5.11) is solar-model independent result putting existing solar models to the test. It shows excellent agreements with ^{8}B flux predicted by BP2000 and the Turck-Chieze *et. al.* SSM's.

The recently reported SNO's results are:

$$\phi^{CC}_{SNO}(\nu_e) = (1.76^{+0.06}_{-0.05} \pm 0.09) \times 10^6 \text{ cm}^{-2}\text{s}^{-1}, \tag{5.12}$$

$$\phi^{ES}_{SNO}(\nu_x) = (2.39^{+0.24}_{-0.23} \pm 0.12) \times 10^6 \text{ cm}^{-2}\text{s}^{-1}, \tag{5.13}$$

$$\phi^{NC}_{SNO}(\nu_x) = (5.09^{+0.44+0.46}_{-0.43-0.43}) \times 10^6 \text{ cm}^{-2}\text{s}^{-1}. \tag{5.14}$$

The deduced fluxes $\phi(\nu_e)$ and $\phi(\nu_{\mu \text{ or } \tau})$ are very well-consistent with SSM (see Figure 5.7). The resultant $\phi(\nu_{\mu \text{ or } \tau})$ is:

$$\phi(\nu_{\mu \text{ or } \tau}) = (3.41^{+0.45+0.48}_{-0.45-0.45}) \times 10^6 \text{ cm}^{-2}\text{s}^{-1}, \tag{5.15}$$

providing much better evidence for neutrino oscillation than equation (5.9).

Beside SNO-SK explanation, many "pre-SNO" solutions of the solar neutrino data in the terms of two-neutrino oscillations exist [2, 4, 5, 6, 31]. Bahcall, Krastev and Smirnov found at 99.7 % CL eight allowed discrete regions in the two-neutrino oscillation space: (1) five active-neutrino solutions: LMA (= Large Mixing Angle), SMA (= Short Mixing Angle), LOW (= LOW probability or LOW mass), VAC and Just So^2 (both vacuum oscillations), (2) three sterile-neutrino solutions: SMA(sterile), VAC(sterile) and Just So^2(sterile).

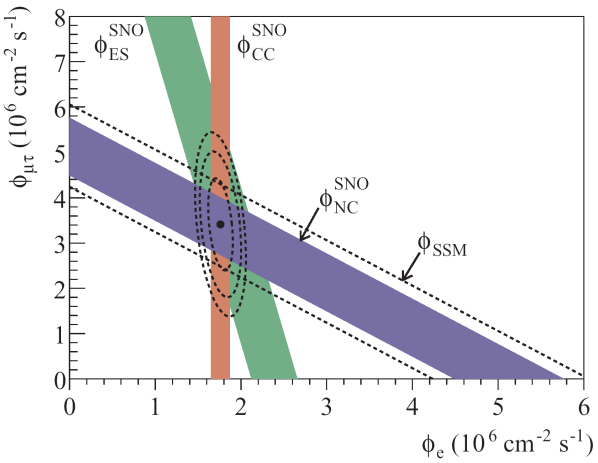

Figure 5.7: The flux of ν_μ and ν_τ versus flux of ν_e in the ^{8}B energy range deduced from three neutrino reactions in SNO. The dashed line diagonal bands show the total ^{8}B flux as predicted by SSM and the solid ones show the flux measured by SNO. The intercepts of these bands with the axes represent the $\pm 1\sigma$ errors. The bands intersect at the fit values for $\phi_e \equiv \phi_{\nu_e}$ and $\phi_{\mu\tau} \equiv \phi_{\nu_{\mu,\tau}}$, ref. [35].

Solution	Δm^2 (eV^2)	$\tan^2\theta$
LMA	4.2×10^{-5}	0.26
SMA	5.2×10^{-6}	5.5×10^{-4}
LOW	7.6×10^{-8}	0.72
VAC	1.4×10^{-10}	0.38
Just So^2	5.5×10^{-12}	1.0

Table 5.3: The best-fit results of the solar neutrino problem models, ref. [31].

The best-fit results for active neutrino solutions are listed in Table 5.3, while the sterile ones are similar to the corresponding active-neutrino solutions.

After analysis of all available and valuable solar neutrino data, LMA, LOW and VAC became the best models . Taking into account the KamLAND results [4], the best solution of all mentioned models became LMA-MSW (LMA taking into account the MSW effect) solution. The future expected result, which could determine the correctness of this theoretical model, will be from Borexino experiment [31].

Chapter 6

Supernova neutrinos

The supernovae (SNe) are the overwhelmingly powerful explosions terminating the life of some types of stars, when several solar masses of their original matter (containing heavy elements important for the chemical evolution of the galaxies, stars, planets and life) is ejected in the interstellar space with the total kinetic energy higher than 10^{45} joules during several seconds. The after-explosion conditions can help to form the new stars, whereas some SNe produce a compact remnant, neutron stars or black holes [4].

Date	Length of visibility	Remnant	Historical records				
			Chinese	Japanese	Korean	Arabic	European
AD1604	12 months	G4·52 6·8	few	-	many	-	many
AD1572	18 months	G120·12 2·1	few	-	two	-	many
AD1181	6 months	3C58	few	few	-	-	-
AD1054	21 months	Crab Nebula	many	few	-	one	-
AD1006	3 years	SNR327·62 14·6	many	many	-	few	two
AD393	8 months	-	one	-	-	-	-
AD386?	3 months	-	one	-	-	-	-
AD369?	5 months	-	one	-	-	-	-
AD185	8 or 20 months	-	one	-	-	-	-

Table 6.1: The summary of the supernovae registered in the past and the sources of their records, ref. [37].

Thanks to many historical records, it is known that several SNe were observed in both millenia of our epoch (see Table 6.1). Nowadays, SNe serves, apart of other things, as sources of neutrinos.

6.1 Supernova types and rates

SNe are divided into two large categories Type I (SNI) and Type II (SNII) characterized by the absence or the presence of hydrogen, respectively [4, 38]. For historical reasons, they are subdivided into four types Ia, Ib, Ic and II differing by their spectrum shapes (see Figure 6.1) reflecting the composition of the SN progenitor star envelope (see Table 6.2).

Typically, the optical emission of the both SN types rise in luminosity during a week or two, when their luminous surface expands. SNeI have a narrow luminosity peak, while SNeII have broad peaks of the order of 100 days. After the peak, the luminosity decreases for about one year (see Figure 6.1).

SNeIa are expected to be generated by carbon-oxygen white dwarfs having a close companion star, whose mass they accrete. As soon as the white dwarf reaches the Chandrasekhar limit 1.4 $M_\odot$ (having a density of order of 10^6 g cm^{-3}), the degenerate electron

Type	near maximum			months later		Mechanism	Remnant
	H	He	Si	Fe	O and C		
Ia	No	No	Yes	Yes	No	Mass Accretion	None
Ib		Yes	No	No	Yes	Core-Collapse	Neutron Star or Black Hole
Ic		No	No				
II	Yes	?	?				

Table 6.2: The main characteristics of SN types, ref. [4].

gas pressure cannot sustain the gravitational weight and the white dwarf begins collapse, triggering the fusion of C and O to the heavier nuclei that liberates an enormous quantity of energy causing the star explosion that disrupts the progenitor white dwarf and generate expanding nebula (”dust” cloud) without a central compact object.

For neutrino physics, SNeIb, Ic and especially SNeII are more important because of their huge all flavor neutrino flux production. SNeII are generated by the core-collapse of the red or blue (SN1987A) giants with masses between 8 and 60 solar masses. The visible explosion effect of collapse varies in a wide range (independently of envelope composition), thus, further subclassification of SNII was developed. SNII-L shows the luminosity decrease almost linear in time, while SNII-P shows a plateau lasting 2-3 months in the luminosity time evolution. SNeIIF are of very low luminosity, in SNeIIb the abundance of helium predominates the hydrogen. SNeIIn have the spectrum showing the narrow line emissions, while SNeIIpec have the peculiar characteristics, but the intermediate cases between all these types exist [4, 38].

A very important problem is the estimate of SN rates. The SNIb, Ic and II rates are dependent on the galaxy type, being very small in very old elliptical galaxies having less short-lived massive stars ending their life via the core-collapse followed by SN explosion, whereas the mass accretion (SNeIa) can occur also in old star formations. Our Milky Way is of the spherical type and the predictions give the rate about 2 ± 1 per century but not much higher. Thus, the possibility of studying some nearby SN is rare [4].

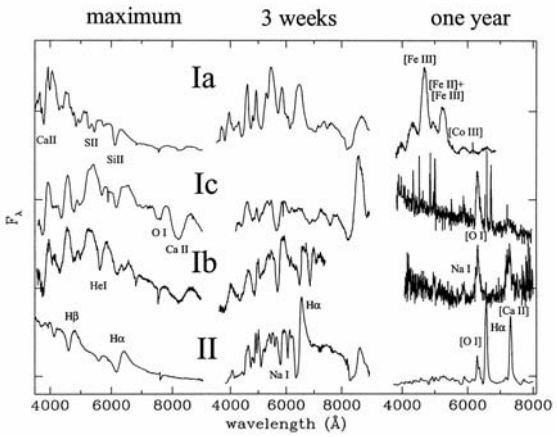

Figure 6.1: The spectra of the main SN types at maximum, three weeks, and one year after maximum. The representative spectra are those of SN1996X for type Ia, of SN1994I (left and center) and SN1997B (right) for type Ic, of SN1999dn (left and center) and SN1990I (right) for type Ib, and SN1987A for type II, ref. [38].

6.2 Supernova neutrino production dynamics

In this section, the core-collapse model well--fitting for SNIb, Ic and SNII with a scenario of the neutron star generation will be shortly described [4].

As mentioned above, the core-collapse is the final phase of the life of stars with masses $8\ M_\odot \lesssim M \lesssim 60\ M_\odot$; the lighter stars become the white dwarfs, while the heavier ones are unstable, ending as the black holes without the SN explosion. Stars with mass $M \gtrsim 12\ M_\odot$ undergo all the stages of nuclear fusion of H, He, C, Ne, O and Si (see Table 6.3), until the star has an onion-like structure (see Figure 6.2) having iron core with mass of about $1\ M_\odot$, a radius of several thousand kilometres, central density of 10^{10} g cm^{-3}, central temperature ~ 1 MeV ($\approx 1\times10^{10}$ K), and its weight sustained by the degenerate relativistic electron pressure.

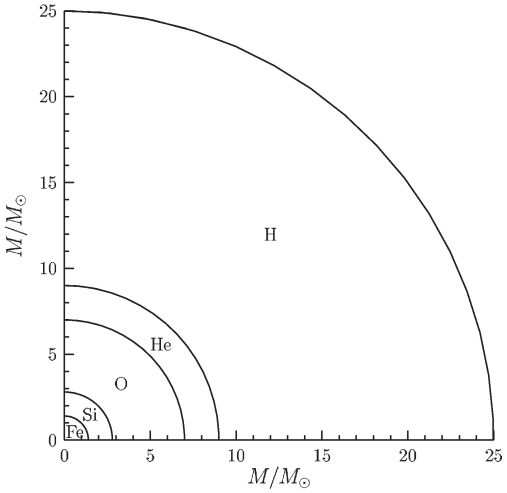

Figure 6.2: The onion-like interior of the star before the collapse, ref. [4].

Furthermore, there is no more thermonuclear fuel to burn and the core becomes endothermic - it can only absorb energy by breaking into lighter nuclei; creating heavier elements is in this moment already impossible. Shortly before reaching the Chandrasekhar mass, the core equilibrium is broken, core contracts and the increasing temperature causes the photodissociation of iron via

$$^{56}\mathrm{Fe} + \gamma \rightarrow 13\alpha + 4n - 124\ \mathrm{MeV}, \tag{6.1}$$

reducing the electron pressure and kinetic energy. Moreover, the electron capture of nuclei (6.2) and free protons (6.3) reduce the electron number and influence:

$$A(Z,N) + e^- \rightarrow A(Z-1, N+1) + \nu_e, \tag{6.2}$$

$$p + e^- \rightarrow n + \nu_e. \tag{6.3}$$

These effects reduce the electron pressure, which is unable to sustain the core weight any more and the collapse begins. The core density and the temperature increase, processes (6.1) - (6.3) proceed faster with lowering the electron pressure and the collapse accelerates.[1] Originating "non-thermal" neutrinos with energy $12\ \mathrm{MeV} \lesssim E_{\nu_e} \lesssim 16\ \mathrm{MeV}$ leave freely the core, carrying away energy and lepton number. The luminosity reaches $\sim 10^{46}$ joules per second, but this process lasts less than 10 ms, thus, only 1 % of total energy is released.

When the density of the core inner part exceeds $\sim 3\times10^{11}$ g cm^{-3} ($M \simeq 0.8\ M_\odot$), neutrinos are caught in the collapsing material leading to an adiabatic collapse with constant lepton number (so-called "catching phase"). During this phase, the inner core collapses with the subsonic velocity proportional to radius, while the outer-core part collapses with supersonic free-fall velocity. About one second later, the density of the nuclear matter is $\sim 10^{14}$ g cm^{-3} and the degenerate non-relativistic nucleon pressure rapidly stops the collapse. The inner-core settles into the hydrostatic equilibrium forming a proto-neutron star (radius of about 10 km), while the supersonic shock wave, caused by inner-core collapse halting, forms at the surface, and propagates outwards through the

[1] In the case of the stars with mass $8\ M_\odot \lesssim M \lesssim 12\ M_\odot$, only H, He and C can be burnt, but the core temperature is insufficient for O-burning. On the other hand, core contains abundant amount of Ne and Mg, reducing electron pressure on the core via (6.2), leading to core-collapse with O, Ne, Mg conversion into Fe. Also in this case, the star ends by the SN explosion caused by the iron core-collapse, as well [4].

Phase	$1\ M_\odot$			$25\ M_\odot$		
	T_c (keV)	ρ_c (g cm^{-3})	Δt (yr)	T_c (keV)	ρ_c (g cm^{-3})	Δt (yr)
H burning	1.3	153	1.1×10^{10}	3.3	3.8	6.7×10^{6}
He burning	11	2.0×10^{4}	1.1×10^{8}	17	762	8.4×10^{5}
C burning				72	1.3×10^{5}	522
Ne burning				135	4.0×10^{6}	0.89
O burning				180	3.6×10^{6}	0.40
Si burning				314	3.0×10^{7}	2.0×10^{-3}

Table 6.3: The evolutionary phases of stars with initial masses $1\ M_\odot$ and $25\ M_\odot$. The central temperature T_c, the central density ρ_c and the time scale Δt of each phase are listed, ref. [4].

outer-core (which is still collapsing) with an initial velocity of the order of 100 km ms^{-1}. The gas that infalls at almost free-fall velocity is rapidly decelerated within the shock and slowly accretes the proto-neutron star surface.

As the shock propagates through the infalling dense outer-core matter, its energy dissipates due to photodissociation of nuclei into protons and neutrons, while free protons interact with electrons, thus, many neutrons together with ν_e's originate. These neutrinos are accumulated behind the shock, which is dense and opaque to them, until the shock reaches a zone ("neutrinosphere") with a density of 10^{11} g cm^{-3} in several milliseconds after bounce ("shock breakout"). Then ν_e's are released in several millisecond (so-called "prompt ν_e burst", different from the thermal all-flavor neutrino production). This prompt ν_e burst carries away an energy of order of 10^{44} joules during several milliseconds; in this moment only the low-density periphery of the proto-neutron star is neutronized.

The energy lost by photodissociation of nuclei and ν-emission weakens the shock ($\sim 1.5\times10^{44}$ joules dissipate for each 0.1 $M_\odot$ of photodissociated material). In the so-called "prompt" SN explosion scenario, the shock, although weakened, is able to expel the envelope of the star, generating the SN explosion during next some 100 ms. If the star mass is $M > 10\ M_\odot$, the shock is both weakened and delayed $\sim$ 100 ms after bounce at the radius of 200-300 km with the insufficient energy to reach the outer star layer. Matter continues falling through the delayed shock and photodissociates. If too much matter settles on the proto-neutron star, the collapse continues finishing by forming the black hole with no explosion.

For continuing the shock, which leads to explosion, some mechanism renewing its energy is needed. There is an idea that the energy is deposited by the huge neutrino flux, which is produced thermally in the proto-neutron star. Then a so-called "delayed" SN explosion is produced during several 100 millisecond after bounce. Neutrinos of all flavors, produced in proto-neutron star core (having temperature about 40 MeV, that is $\approx\ 5\times10^{11}$ K), originate through electron-positron annihilation ($e^+ + e^- \to \nu + \bar{\nu}$), electron-nucleon bremsstrahlung ($e^\pm + N \to e^\pm + N + \nu + \bar{\nu}$), nucleon-nucleon bremsstrahlung ($N + N \to N + N + \nu + \bar{\nu}$), plasmon decay ($\gamma \to \nu + \bar{\nu}$) and photoannihilation ($\gamma + e^\pm \to \nu + \bar{\nu}$), as well as ν_e's are also produced via (6.3) and $\bar{\nu}_e$'s via positron capture on neutron ($e^+ + n \to p + \bar{\nu}_e$).

As mentioned above, there exists the neutrinosphere in mantle of the proto-neutron star, outwards from which neutrinos can leave the dense inner matter. Since the neutrino interactions depend on flavor and energy, there are different energy dependent ones for each ν-flavor (estimated radii of neutrinospheres lie between 50 and 100 km). Since the medium consists of protons, neutrons and electrons, and ν-energy does not allow the μ or τ creation, ν_e and $\bar{\nu}_e$ can interact with medium via both CC and NC reactions, whereas

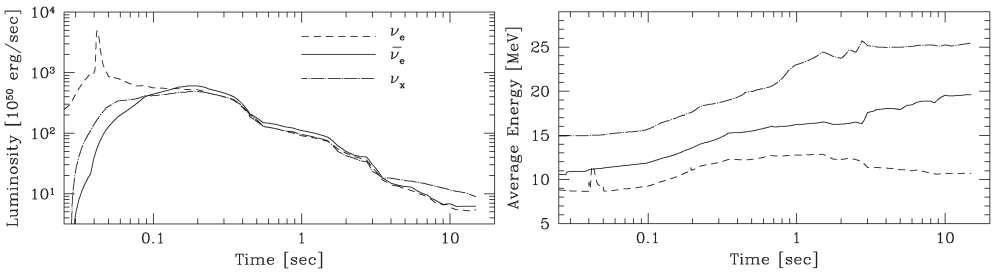

Figure 6.3: The numerical model of the time evolution of neutrino luminosity and energy. A luminosity and energy peak represents the "prompt ν_e burst". ν_x means ν_μ, ν_τ and their antiparticles, ref. [4].

ν_μ, $\bar{\nu}_\mu$, ν_τ, $\bar{\nu}_\tau$ interact only via (flavor independent) NC processes.

Opacities of ν_e's and $\bar{\nu}_e$'s are dominated by the CC reactions ($\nu_e + n \rightarrow p + e^-$, $\bar{\nu}_e + p \rightarrow n + e^+$), thus, these reactions allow energy and lepton number exchange between neutrinos and medium. Since the mantle of proto-neutron star is neutron-rich, the opacity of ν_e's with given energy is larger than the opacity of $\bar{\nu}_e$'s with the same energy, thus, the corresponding ν_e-sphere has larger radius than $\bar{\nu}_e$-sphere. Accordingly for a fixed ν-energy, $\bar{\nu}_e$'s are emitted from a deeper and hotter layers than ν_e's. It leads to a fact that average $\bar{\nu}_e$-energy is higher than ν_e-one [4]:

$$\langle E_{\nu_e} \rangle \approx 10 \text{ MeV}, \quad \langle E_{\bar{\nu}_e} \rangle \approx 15 \text{ MeV}, \quad \langle E_x \rangle \approx 20 \text{ MeV}. \tag{6.4}$$

6.3 SN1987A

On 23 February 1987, at 7:35 UT, a very bright Type II supernova, SN1987A, was discovered in the Large Magellanic Cloud at a distance of about 50 kpc ($\approx 1.54 \times 10^{18}$ km). At that time, four large underground neutrino detectors were in the operation: Kamiokande-II (12 events, $\Delta t = 12.5$ s, $\langle E \rangle \simeq 14.7$ MeV), IMB (8 events, $\Delta t = 5.6$ s, $\langle E \rangle \simeq 31.9$ MeV), Baksan (5 events, $\Delta t = 9.1$ s, $\langle E \rangle \simeq 18.1$ MeV), recording data in the same time, and excluded LSD experiment (registered some events 5 hours before the others) [4].

SN1987A is the best studied of all SNe not only because of the detection of its neutrinos; it was, as well, visible to the naked eye, and moreover, its progenitor star is known (blue supergiant B3 I S Sanduleak - 69°202). The SN1987A remnant evolution was studied in all spectral bands, and although no compact object was identified, at present, some indications of the 2.14 ms optical pulsar exist. This SN meant the beginning of the extra solar system neutrino astronomy and as it was one of a great achievements of the Kamiokande project, its designer Masatoshi Koshiba won the Nobel Prize in 2002.

The analysed data [4] showed, that the delayed explosion mechanism is a hundred times more probable than the prompt one. The average $\bar{\nu}_e$-energy was about 15 MeV. The cooling of the proto-neutron star took about 4 seconds, whereas the accretion component took about 0.7 seconds. The total number of $\bar{\nu}_e$'s emitted was $\sim 3 \times 10^{57}$ (about 10^{28} ν's passed through Earth), the binding energy ΔE_B of the neutron star given by:

$$\Delta E_B \sim \frac{\varkappa M_{core}^2}{R} = 3 \times 10^{46} \left(\frac{M_{core}}{M_\odot} \right)^2 \left(\frac{R_{NS}}{10 \text{ km}} \right)^{-1} \text{joules}, \tag{6.5}$$

where $\varkappa$ is Newton gravitational constant, M_{core} is the core mass and R_{NS} is the radius of the originated neutron star, was approximately 3×10^{46} joules.

6.4 Experimental status

6.4.1 Neutrino properties obtained from supernova experiments

The mass of neutrinos from SNe is bounded by:

$$m_\nu \lesssim E\sqrt{\frac{E}{\Delta E}\frac{\Delta T_{obs}}{D}} \simeq 14\ \mathrm{eV}\left(\frac{E}{10\ \mathrm{MeV}}\right)\sqrt{\frac{E}{\Delta E}}\left(\frac{T_{obs}}{10\ \mathrm{sec}}\right)^{1/2}\left(\frac{50\ \mathrm{kpc}}{D}\right)^{1/2}, \tag{6.6}$$

where E is the average value of neutrino energy spectrum, ΔE is the width of neutrino energy spectrum, T_{obs} is the observation time interval of the neutrino burst and D represents the distance between SN and Earth [4]. The $\bar{\nu}_e$-mass extent is $m_{\bar{\nu}_e} \lesssim 8-30$ eV, while applying special statistical method the result is $m_{\bar{\nu}_e} < 5.7$ eV. In the case of neutrino oscillations, no special results occur and the three-flavor model with $m^2_{sol} \approx 5\times 10^{-5}\mathrm{eV}^2$ and $m^2_{atm} \approx 2.5\times 10^{-3}\mathrm{eV}^2$ is valid.

Analyses of SN1987A data bound the neutrino life time by $\tau_{\bar{\nu}_e} \gtrsim 1.6\times 10^5\left(\frac{m_{\bar{\nu}_e}}{E_{\bar{\nu}_e}}\right)$ yr. More, the total amount of emitted energy predicted from $\bar{\nu}_e$-flux measurement is compatible with the binding energy of the neutron star, only if the number of neutrinos is $N_\nu \lesssim 6$ (that supports LEP result [1]). The observed 10 s timescale of cooling of the proto-neutron star implies the upper magnetic momentum of ν_e's $\mu_{\nu_e} \lesssim 10^{-12}\mu_B$ (if some (right-handed) sterile neutrino exists, the cooling must last less than 1 second). And finally, the limit for electron neutrino electric charge is $q_{\nu_e} \lesssim 10^{-17}e$ [4].

6.4.2 Experiments

Several experiments sensitive to SN neutrinos currently operate (SK [39], SNO [40], KamLAND, ...) or are under preparation (see Appendix 1). Present detectors are as large as they can register about 10^4 events during SN explosion, thus, the SN dynamics can be studied in more detail, but for neutrino properties, some experimental limits exist. The first is, that the direct kinematic tests will not give better results of ν-mass than 0.2 eV (KATRIN [8]). The second problem is, that although fluxes of each neutrino type are of the same order, they can be completely observed only via NC reactions giving no information about ν-flavor (energy is too low for production of μ's or τ's in CC processes), thus, the muon and tau neutrino fluxes can only be separated statistically. Furthermore, the usual NC reaction ($\nu + {}^2\mathrm{H} \rightarrow p + n + \nu$) does not determine the ν-energy, and ν_μ- and ν_τ-energy cannot be below 30 eV. Finally, maybe the main disadvantage is the low SN rate in the Milky Way (only 2 ± 1 per century).

One of the hopeful ways may be the study of the ν-signal due to black hole formation, which may decrease a sensitivity to ν_μ and ν_τ to about 6 eV. Another way is, the recoil proton kinetic energy of order of 1 MeV in NC neutrino-proton elastic scattering ($\nu + p \rightarrow \nu + p$) can be measured (by the scintillator detectors - KamLAND, BOREXINO) to determine the neutrino temperature (important for the universe evolution) and the total neutrino energy with 10 % accuracy.

Conclusion

The neutrino physics is a very important part of the contemporary science. Its results concern the particle and experimental physics, the cosmology as well as the modern view of the evolution of our Universe.

The purpose of this review was to summarize the latest results of the several different branches of neutrino physics and to present the most important experiments in this field.

As well, this work serves as a way to acquaint the author with the formalism and the phenomenology used in this field of physics. That is the reason, why some parts contain more detailed description of both theory and experiments.

Appendix 1: Neutrino experiments

Name	St	Ac	At	As	ν_e	ν_μ	ν_τ	BD	Re	So	SN	WWW
AMANDA	o			✗							✗	http://amanda.berkeley.edu/amanda/amanda.html
ANTARES	f			✗								http://antares.in2p3.fr/
Baksan	o		✗								✗	http://www.inr.ac.ru/INR/Baksan.html
Baikal	o			✗							✗	http://www.inr.ac.ru/INR/Baikal.html
BNL Neutrino Working Group	o	✗										http://minos.phy.bnl.gov/nwg
BooNE	o	✗									✗	http://www-boone.fnal.gov/
BOREXINO	o									✗		http://almime.mi.infn.it/
Bugey	o								✗			http://www.unine.ch/phys/corpus/MUNU/MUNU2.html
CAMEO (^{116}Cd)	f							✗				
CANDLES (^{48}Ca)	f							✗				
CCFR	o	✗				✗						http://www.nevis.columbia.edu/ccfr/
CDHSW	o	✗				✗						http://niceww.cern.ch/ knobloch/CDHS/cdhs.html
CERN-PS-191	o	✗										http://www.cern.ch/
CHOOZ	o								✗			http://www.pi.infn.it/chooz
CHORUS	o	✗										http://choruswww.cern.ch/
COBRA (^{130}Te)	f							✗				
COSMOS	o	✗										http://pooh.physics.lsa.umich.edu/e803/e803.html
CUORE, Cuoricino (^{130}Te)	f							✗				http://crio.mib.infn.it/wig/
DCBA (^{150}Nd)	f							✗				
DONUT	o						✗					http://fn872.fnal.gov/
ELEGANT	f							✗				
EXO (^{136}Xe)	f							✗				http://hep.stanford.edu/neutrino/EXO
GALLEX (^{51}Cr ν source)	o									✗		http://www.mpi-hd.mpg.de/kirsten/gallex.html
Gargamelle	o	✗										
GEM (^{76}Ge)	f							✗				
GENIUS (^{76}Ge)	f							✗				http://www.mpi-hd.mpg.de/non_acc/genius.html
Genova ^{187}Re ν_e-Mass	o				✗							http://www.ge.infn.it/~opisso/vitale.html
GNO	o									✗		http://www.lngs.infn.it/site/exppro/gno/Gno_home.htm
Gosgen	o								✗			
Gotthard (^{136}Xe)	o							✗				http://www.unine.ch/phys/corpus/Gothard/got_art.html
GSO (^{160}Gd)	f							✗				
Heidelberg-Moscow (^{76}Ge)	o							✗				http://www.mpi-hd.mpg.de/non_acc/dblbeta.html
HERON	f									✗		http://www.physics.brown.edu/research/cme/heron/
Homestake	o									✗		http://www.nusl.org/
ICARUS	o,f	✗									✗	http://pcnometh4.cern.ch/
IceCube	f			✗								http://icecube.wisc.edu/
IGEX (^{76}Ge)	o							✗				
IHEP-JINR	o	✗										
ILL	o	✗										
IMB	o		✗								✗	http://www.phys.cmu.edu/~clark/imb.html
JHF-Kamioka	o	✗										http://neutrino.kek.jp/jhfnu
K2K	o	✗										http://neutrino.kek.jp/
Kamiokande	o		✗									http://www-sk.icrr.u-tokyo.ac.jp/doc/kam/index.html
KamLAND	o								✗			http://www.awa.tohoku.ac.jp/html/KamLAND/index.html
KARMEN	o	✗										http://www-ik1.fzk.de/www/karmen/karmen_e.html
KATRIN ν_e-Mass	f				✗							http://ik1au1.fzk.de/~katrin
Kamiokande	o									✗	✗	http://www-sk.icrr.u-tokyo.ac.jp/doc/kam/index.html
KamLAND	o	✗									✗	http://www.awa.tohoku.ac.jp/html/KamLAND
Krasnoyarsk	o								✗			
LAND	f										✗	http://www.neutrino.bnl.gov/
LENS	o									✗		http://www.mpi-hd.mpg.de/lens/www_lens_mpik/lens_physics.htm
LSND	o	✗										http://www.neutrino.lanl.gov/LSND
LVD	o										✗	http://www.lngs.infn.it/site/exppro/lvd/lvd.html
MACRO	o		✗									http://www.lngs.infn.it/site/exppro/macro/macro.html
Mainz ν_e-Mass	o				✗							http://www.physik.uni-mainz.de/exakt/neutrino/en_index.html
Majorana (^{76}Ge)	f							✗				http://majorana.pnl.gov/
MIBETA (^{130}Te)	o							✗				
MiniBooNE	o	✗										http://www-boone.fnal.gov/
MINOS	o	✗										http://www-numi.fnal.gov/
MONOLITH	o		✗									http://www.to.infn.it/monolith/
MOON (^{100}Mo)	f							✗				http://ewi.npl.washington.edu/moon
MUNU	o				✗							http://www.unine.ch/phys/corpus/MUNU/MUNU2.html
NEMO (^{100}Mo, ^{82}Se)	o							✗				http://www.lal.in2p3.fr/recherche/nemo
NESTOR	o		✗	✗							✗	http://www.nestor.org.gr/
NOE	o	✗										http://www1.na.infn.it/wsubnucl/accel/noe/noe.html
NOMAD	o	✗										http://nomadinfo.cern.ch/
NUSEX	o		✗									
NuTeV	o	✗				✗						http://www-e815.fnal.gov/
OMNIS	f										✗	http://www.physics.ohio-state.edu/OMNIS
OPERA	o	✗										http://operaweb.web.cern.ch/operaweb
ORLaND	o	✗							✗			http://www.phys.subr.edu/orland/
P929	o	✗										http://www-off-axis.fnal.gov/
Palo Verde	o								✗			http://citnp.caltech.edu/PV/Palo-Verde.html
RAND	o		✗	✗							✗	http://aether.lbl.gov/www/projects/neutrino/rand/rand.html
RICE	o			✗							✗	http://kuhep4.phsx.ukans.edu/~iceman/
Rovno	o								✗			
SAGE	o									✗		http://ewi.npl.washington.edu/SAGE/sage.html
Savannah River	o								✗			
SNO	o									✗	✗	http://www.sno.phy.queensu.ca/
Soudan 2	o		✗									http://hepunx.rl.ac.uk/soudan2
Super-Kamiokande	o		✗							✗	✗	http://www-sk.icrr.u-tokyo.ac.jp/doc/sk/index.html
TEXONO ν_e-Mass	f				✗							http://hepmail.phys.sinica.edu.tw/~texono
TOSCA	f	✗										http://www.cern.ch/TOSCA/
Troitsk ν_e-Mass	o				✗							http://www.inr.troitsk.ru/~trdat
UNO	f										✗	http://superk.physics.sunysb.edu/nngroup/uno/main.html
XMASS (^{136}Xe)	f							✗				

Notes:
St ... Present status of experiment
o ... Experiment in operation/finished
f ... Future experiment
Ac ... Accelerator experiment
At ... Atmospheric neutrino experiment
As ... Astrophysical neutrino experiment
ν_e ... ν_e-property experiment
ν_μ ... ν_μ-property experiment
ν_τ ... ν_τ-property experiment
BD ... $\beta\beta$-decay experiment
Re ... Reactor experiment
So ... Solar neutrino experiment
SN ... Supernova neutrino experiment
WWW ... Experiment home page

Appendix 2: Short neutrino history

Everything began in February 1896. After the discovery of the X-rays by Wilhelm C. Röntgen (Nobel Prize in 1901) in 1895, Antoine H. Becquerel (Nobel Prize in 1903) made a test to reveal if a radiation emanated by fluorescent materials, mainly the often used uranium salts, is the same as X-rays or not. Becquerel put a piece of uranium on a photographic plate covered by a black paper and after developing it, he found out that the place under the uranium became black. Originally the Becquerel's radiation was renamed as radioactivity by Marie Curie in 1898 and went to detailed study.


A. H. Becquerel


E. Rutherford


L. Meitner


O. Hahn


N. H. D. Bohr

As early as in 1899, Ernest Rutherford found out that there existed two different kinds of radioactivity: one represented by a positively-charged "alpha" and the other by a negatively-charged "beta" particles. One year later, Paul U. Villard discovered, in addition, the third type of radioactivity unaffected by the magnetic field. Rutherford found out, that this one is represented by the electromagnetic waves and called it "gamma" radioactivity. Pierre and Marie Curie (both winners of the Nobel Prize in 1903) made in 1902 further discovery finding out that β radioactivity is a current of electrons. In this year, as well, Frederick Soddy and Rutherford observed, that α and γ radioactivity have a different substance and finally, in 1904, Rutherford showed that α radioactivity is nothing more than the current of helium nuclei ("helions").

Very important discovery, besides the discovery of the proton by Rutherford in 1910 and several new chemical elements, made James Chadwick. In 1914, he found out, on basis of the preceding works of Lise Meitner and Otto Hahn, that β radioactivity has a continuous energy spectrum. Niels H. D. Bohr supported his result but other physicists expected that electrons have one or several discrete energies corresponding to the energy of the nuclear transitions.

Only in 1930 (when Paul A. M. Dirac (Nobel Prize in 1933) predicted the existence of antimatter and Ernest O. Lawrence (Nobel Prize in 1939) constructed the first cyclotron), Wolfgang Pauli (Nobel Prize in 1945) solved this inexplicable problem. To explain the apparent energy nonconservation in radioactive decay, he proposed that a neutral particle was emitted, unseen, together with the electron, carrying away the missing energy from a detector. The 4th of December 1930, Pauli presented this idea in the letter addressed to his colleagues at a workshop in Tübingen.

> Dear Radioactive Ladies and Gentlemen.
>
> As the bearer of these lines, to whom I graciously ask you to listen, will explain to you in more detail, how because of the "wrong" statistics of the N and Li6 nuclei and the continuous beta spectrum, I have hit upon a desperate remedy to save the "exchange theorem" of statistics and the law of conservation of energy. Namely, the possibility that there could exist in the nuclei electrically neutral particles, that I wish to call neutrons, which have spin 1/2 and obey the exclusion principle and which further differ from light quanta in that they do not travel with the velocity of light. The mass of the neutrons should be of the same order of magnitude as the electron mass and in any event not larger than 0.01 proton masses. The continuous beta spectrum would then become understandable by the assumption that in beta decay a neutron is emitted in addition to the electron such that the sum of the energies of the neutron and the electron is constant. . .
>
> I agree that my remedy could seem incredible because one should have seen those neutrons very earlier if they really exist. But only the one who dare can win and the difficult situation, due to the continuous structure of the beta spectrum, is lighted by a remark of my honoured predecessor, Mr Debye, who told me recently in Bruxelles: "Oh, It's well better not to think to this at all, like new taxes". From now on, every solution to the issue must be discussed. Thus, dear radioactive people, look and judge. Unfortunately, I cannot appear in Tübingen personally since I am indispensable here in Zurich because of a ball on the night of 6/7 December. With my best regards to you, and also to Mr Back.
>
> Your humble servant
> W. Pauli

Two years later, Chadwick (Nobel Prize in 1935) discovered a new particle "neutron" but it was too heavy to correspond to the particle Pauli imagined. In this year, as well, Carl D. Anderson

discovered in cosmic rays (discovered by Victor F. Hess (Nobel Prize in 1936) in 1911) the positrons (the first proof the Dirac's theory of antimatter was true). At Solvay conference in Bruxelles, in October 1933, Pauli presented his results and ideas about his particles: *"... their mass can not be very much more than the electron mass. In order to distinguish them from heavy neutrons, mister Fermi has proposed to name them neutrinos*[2]*. It is possible that the proper mass of neutrinos be zero... It seems to me plausible that neutrinos have a spin 1/2... We know nothing about the interaction of neutrinos with the other particles of matter and with photons: the hypothesis that they have a magnetic moment seems to me not funded at all."*

Further problem was connected with the character of neutrino. If an antiparticle of neutrino (antineutrino) exists, the question was, whether neutrino and antineutrino are two different particles (Dirac case) or whether neutrino and its antiparticle are identical ones (Majorana case; Ettore Majorana). Until today, it is not clear (more in section 1.2) .

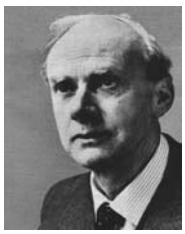
P. A. M. Dirac


W. Pauli


J. Chadwick


C. D. Anderson


E. Fermi

In the same year, it was shown that neutrino mass has to be much lower than the electron mass, as well as Fréderic J. Curie discovered β^+ radioactivity. On the basis of these experiments, Enrico Fermi (Nobel Prize in 1938) formulated a comprehensive theory of β decay, which included Pauli's hypothetical particle. This theory involved a new reaction in which the neutron changes into a proton, electron and an antineutrino

$$n \rightarrow p + e^- + \bar{\nu}.$$

On the basis of the Fermi's theory, in 1934, Hans A. Bethe (Nobel Prize in 1967) and Rudolf Peierls calculated an interaction cross section for neutrino reactions

$$\nu + n \rightarrow e + p,$$
$$\bar{\nu} + p \rightarrow e^+ + n.$$

For neutrino energy of 1 MeV the cross section came out less than 10^{-43} cm^2, so the detection of neutrinos seemed (experimentally) impossible.

Another important events were the discovery of the muons in cosmic rays by Carl D. Anderson (Nobel Prize in 1936) and Seth H. Neddermeyer in 1936. In 1939, Luis W. Alvarez (Nobel Prize in 1968) discovered radioactive tritium ${}^3_1\mathrm{H}$ (whose β decay gives, until today, good limit of neutrino mass) and in the same year, Bethe and Carl F. Weisäcker separately developed the draft of hydrogen synthesis as the process of the origin of Sun's energy.


E. Majorana

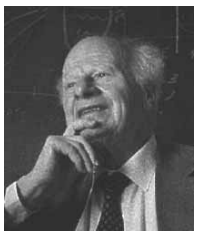
H. A. Bethe


C. F. Weisäcker


F. Reines


C. Cowan

In 1946, Bruno Pontecorvo proposed the reaction for catching neutrinos on Earth:

$$\nu + \mathrm{Cl} \rightarrow \mathrm{Ar} + e^-,$$

[2]Italian: neutrino = "little neutral one"

which was later really used in Homestake experiment. Next year, in 1947, Cecil F. Powell discovered, again in cosmic rays, new particles called pions, which undergo the decay chain $\pi^+ \to \mu^+ \to e^+$. He observed that the π^+ stops and the μ^+ emerges from the stopping point with a unique energy. To conserve momentum, it had to be assumed that an unseen neutral particle was emitted opposite to the μ^+. It was natural to propose that was neutrino. But of which kind, if any?

Not so long after the war nuclear catastrophes in Japan, in 1951, Frederick Reines wanted to use an atomic bomb as a powerful source of neutrinos but, fortunately, he chose another, peaceful way. In 1952, with a help of Clyde Cowan, he decided to use the nuclear plant of Hanford (Washington) as a source. The detector was built quickly, their experiment was proposed in February 1953, realized in spring, but the results presented in summer was not too convincing. They repeated it, in 1956, more carefully near the nuclear plant of Savannah River (South Carolina) using the reaction $\bar{\nu} + p \to e^+ + n$ and thanks to a reduction of the background, they discovered a particle fitting the expected characteristics of the neutrino.

Reines and Cowan experiment principle consisted in using a target made of about 400 liters of a mixture of water and cadmium chloride. The anti-neutrino coming from the nuclear reactor interacts with a proton of the target matter, giving a positron and a neutron. The positron annihilates with an electron of the surrounding material, giving two simultaneous photons and the neutron slows down until it is eventually captured by a cadmium nucleus, implying the emission of photons some 15 μs after those of the positron annihilation. All those photons were detected and the 15 μs identified the neutrino interaction.

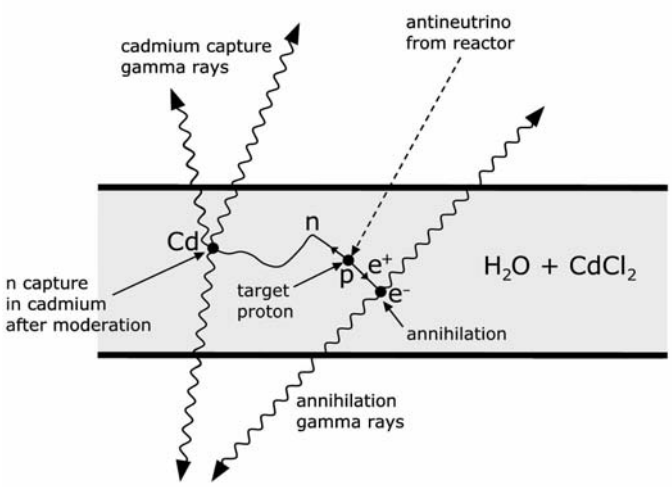

Figure A2.1: Scheme of 1956 experiment, ref. [9].

In analogy with the oscillations $\bar{K}^0 \leftrightarrow K^0$ (Murray Gell-Mann (Nobel Prize in 1969), 1955), Pontecorvo, in 1957, proposed the oscillations $\bar{\nu} \leftrightarrow \nu$ in vacuum.

Another property of neutrino was uncovered in 1958 when Goldhaber, Grodzins and Sunyar demonstrated through the reaction

$$e + {}^{152}\mathrm{Eu} \to {}^{152}\mathrm{Ar}^* + \nu_e,$$

that neutrino has the left-handed helicity (meaning that it spins along the direction of its motion in the sense of a left-handed screw).

During 1960, Tsung D. Lee and Chen N. Yang (both winners of the Nobel Prize in 1957) were more and more convinced that if a reaction $\mu^- \to e^- + \gamma$ is not observed, it is because two types of neutrino exist. As soon as the spark chamber was built at Princeton University, the group of young physicists from Brookhaven National Laboratory (Leon Lederman, Jack Steinberger, Jean-Marc Gaillard) and from Columbian University (T. D. Lee, C. N. Yang, Melvin Schwartz) performed an experiment to prove these two types. The accelerator of Brookhaven delivered some hundreds of millions of neutrinos per hour, among which about forty interacted clearly with the detector. In six cases the particles coming out of interactions were identified as the electrons, the others as the muons. The result was that electron (ν_e) and muon (ν_μ) neutrinos are two different particles. In

addition, this result meant the discovery of ν_μ. Finally in 1988, Steinberger, Lederman and Schwartz wan the Nobel Prize for its discovery.

Between years 1967 and 1969, Bruno Pontecorvo and Vladimir N. Gribov proved the nonconservation of lepton number in β decay and came with theory of oscillations $\nu_e \leftrightarrow \nu_\mu$.

From 1967 to 1972, Sheldon L. Glashow, Abdus Salam and Steven Weinberg (all winners of the Nobel Prize in 1979) created the unified theory of electromagnetic and weak interactions.


L. Lederman


J. Steinberger


T. D. Lee


C. N. Yang


M. Schwartz

The closest gigantic neutrino source is our Sun and Raymond Davis jr. with John Bahcall used it for measurement. In 1967, they installed 600 tons C_2Cl_4 detector in Homestake gold mine (South Dacota) using Pontecorvo's reaction $\nu + \mathrm{Cl} \rightarrow \mathrm{Ar} + e^-$. The first results were published in 1968 but the number of detected neutrinos came out only less than half of the expected number calculated by Bahcall ($\approx$ 2-3/day). Their experiment operated up to 1994 and although the results were continuously put more precisely, they were still similar. That fact started a long-range "solar neutrino problem" based on the deficit in measured number of neutrinos, caused by oscillations of ν_e into another types undetectable by this experiment. Physicists thought, too, that it would be caused by a wrong solar model used for calculating of the rates but till 2002 there was no solution.

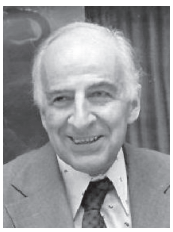
B. Pontecorvo


V. N. Gribov


S. L. Glashow


A. Salam


S. Weinberg

The year 1973 is characterised by two events: the first was the formulation of the Quantum chromodynamics by Gross, Politzer and Wilczek (the basic draft was made by Gell-Mann and Fritzsch in 1970), the other event happened in CERN in Geneva (Switzerland), where, thanks to the bubble chamber called Gargamelle, the first example of a "neutral current"[3] (NC) was observed. This interaction presents a strong support to the unified theory of electroweak interactions proposed by Glashow, Salam and Weinberg.

Two years later, a new τ lepton was discovered by the group led by physicist Martin Perl at Stanford Linear Accelerator Center (SLAC). This new particle guaranteed the Nobel Prize to Perl and Reines in 1995.

In 1978, L. Wolfenstein brought to light the theory of neutrino oscillations in matter. The basic idea was, that the index of refraction of ν_e is different from that of ν_μ due to scattering from electrons and that fact had to be included in quantum-mechanical oscillation equations. This theory was extended by the works of S. P. Mikheyev and A. Y. Smirnov in 1986 and whole phenomenon was called "MSW effect" (see Chapter 3, page 16).

From 1983, a new detector, Kamiokande, in Kamioka mine in Japan began operate. One year later, Kamiokande-II was put into operation. Same year, Carlo Rubbia and Simon van der Meer, working in CERN, proved the existence of $W^\pm$ and Z gauge bosons mediating the weak interaction. In 1984, both wan the Nobel Prize.

During 1988, Kamiokande group reported, that they observe only about 60% of the expected rate of ν_μ. This result was supported, in 1989, by Fréjus and NUSEX experiments. Experiments at

[3] NC = neutrino interaction with the matter where ν is not transformed into another particle (lepton)

CERN's Large Electron Proton (LEP) accelerator and at Stanford showed simultaneously that there can exist only three species of light (or massless) neutrinos. Thus ν_e, ν_μ, ν_τ and their antiparticles must complete this class of particles. This direct measurement verified the strong suggestions previously deduced from the cosmological measurements. Finally, in this year, as well, Kamiokande became the second experiment detecting sun neutrinos and confirmed the long standing anomaly by finding only about 1/3 of the expected rate, which was supported in 1990 by upgraded IMB detector and later by Gallex, Sage and Homestake.


J. Bahcall


C. Rubbia


S. van der Meer

New CERN's experiments for detecting neutrino oscillations (NOMAD and CHORUS) began operate in 1994, with the hope to see some ν_τ inside a beam of ν_μ produced by the protons of the CERN SPS accelerator. But for next six years, yet, they had no significant results. In 1994, as well, Kamiokande and IMB groups collaborated to test the ability of water detectors to distinguish ν_μ and ν_e interactions, using a test beam produced by the KEK accelerator laboratory. The results confirmed the validity of earlier measurements. Later these two groups formed a nucleus of the Super-Kamiokande project beginning operate in 1996, measuring the flux of atmospheric ν_μ and sun ν_e. Measured data were confirmed by LSND (1996) and by another new iron detector Soudan II (1997).

Finally, in August 2000, the third tau neutrino was found by Fermilab's experiment DONUT. The DONUT group consisted of American, Greek, Japanese and South Korean teams from 13 universities. As a source of neutrinos, they used the beam of 800 GeV protons from Fermilab's Tevatron interacting in one metre long tungsten beam dump. Most of the neutrinos that interacted in the emulsion target originated from the decays of charmed mesons in the beam dump. The primary source of ν_τ was the leptonic decay of charmed, strange mesons D_S into τ and $\bar{\nu}_\tau$, and the subsequent decay of the τ to a ν_τ. From 203 analyzed neutrino interactions recorded in the nuclear emulsion targets, a decay search found an evidence of four tau neutrino interactions. The number was consistent with the Standard Solar Model expectation.

The year 2002 was marked by two important occurrences. One, closing of the "solar neutrino problem" (more in section 5.3) and the other, the Nobel prize for Raymond Davis jr. and Masatoshi Koshiba for the pioneering contributions to astrophysics, in particular for the detection of cosmic neutrinos.

This text is based on the references [9, 21, 22, 41, 42, 43, 44, 45].

References

[1] D. Karlen, *Number of neutrino types and sum of neutrino masses*, Phys. Rev. D **66**, 2002.

[2] E. Kh. Akhmedov, *Neutrino physics*, arXiv:hep-ph/0001264, 2000.

[3] K. Hagiwara et. al., *Review of particle physics*, Phys. Rev. D **66**, Particle Data Group, http://pdg.lbl.gov/, 2002.

[4] S. M. Bilenky, C. Giunti, J. A. Grifols, E. Massó, *Absolute values of neutrino masses: Status and prospects*, arXiv:hep-ph/0211462, 2003.

[5] M. H. Shaevitz, *Neutrino physics, masses, and oscillations*, 2002.

[6] K. Zuber, *On the physics of massive neutrinos*, arXiv:hep-ph/9811267, 1998.

[7] Ch. Kraus, *Most recent results of the Mainz neutrino mass experiment*, Nucl. Phys. **B** (Proc. Suppl.) 118 (2003) 482.

[8] KATRIN Collaboration, *KATRIN letter of intent*, arXiv:hep-ex/0109033, 2001.

[9] D. Verkindt, http://wwwlapp.in2p3.fr/neutrinos/aneut.html, 1999.

[10] P. Čermák, *Double beta decay*, Review work (in czech), FNSPE CTU Prague, 1997.

[11] A. S. Barabash, Czech. J. Phys. **52** (2002) 567-581.

[12] H. V. Klapdor-Kleingrothaus, *Latest results from the Heidelberg-Moscow double beta decay experiment*, Eur. Phys. J. A **12** (2001) 147-154.

[13] H. V. Klapdor-Kleingrothaus, *Evidence for neutrinoless double beta decay*, Mod. Phys. **A**, Vol. 16, No. 37 (2001) 2409-2420.

[14] H. V. Klapdor-Kleingrothaus, *Status of evidence for neutrinoless double beta decay*, arXiv:hep-ph/0302248, 2003.

[15] A. S. Barabash, *Current double beta decay experiments*, MEDEX 2003 talk, 2003.

[16] Ch. Brofferio, *World status on double beta decay*, 2002.

[17] J. Gerndt, *Detectors of ionizing radiation*, Lecture notes (in czech), FNSPE CTU Prague, 1996.

[18] NEMO Collaboration, *NEMO, Proposition d'expérience de double désintégration bêta pour la recherche d'une masse de neutrino de Majorana de 0.1 eV.*, Internal report, 1993.

[19] NEMO Collaboration, *NEMO experiment*, 2003.

[20] R. Saakyan, *NEMO-3 $\beta\beta$ experiment. First Results and Future Prospects.*, 2003.

[21] S. M. Bilenky, *Early years of neutrino oscillations*, arXiv:hep-ph/9908335, 1999.

[22] J. Chýla, *Nobel neutrinos* (in czech), 2002.

[23] K. Eitell, *The LSND and KARMEN short baseline accelerator-based neutrino oscillation searches*, 2003.

[24] NOMAD Collaboration, *Search for $\nu_\mu \to \nu_e$ oscillations in the NOMAD experiment*, arXiv:hep-ex/0306037, 2003.

[25] K. Zuber, *Latest CHORUS and NOMAD results*, arXiv:hep-ex/0206006, 2002.

[26] M. Maltonia *et. al.*, *Can four neutrinos explain global oscillation data including LSND & cosmology?*, arXiv:hep-ph/0305312, 2003.

[27] J. Link, *Short baseline neutrino oscillations and MiniBooNE*, 2003.

[28] M. Sorel, *Prospects for sterile neutrino searches in MiniBooNE*, 2003.

[29] R. J. Wilkers, *New results from Super-K and K2K*, arXiv:hep-ex/0212035, 2002.

[30] Ch. Mauger, *Super-Kamiokande: Atmospheric neutrinos*, 2002.

[31] K. Nakamura, *Solar neutrinos*, Phys. Rev. D **66**, 2002.

[32] C. Giunti, M. Laveder, *Essential solar neutrinos*, arXiv:hep-ph/0301276, 2003.

[33] Y. Itow, *Results in neutrino oscillations from Super-Kamiokande I*, 2002.

[34] A. W. P. Poon, *Neutrino observations from the Sudbury Neutrino Observatory*, arXiv:nucl-ex/0110005, 2001.

[35] SNO Collaboration, *Direct evidence for neutrino flavor transformation from neutral-current interactions in the Sudbury Neutrino Observatory*, arXiv:hep-ex/0204008, 2002.

[36] SNO Collaboration, *Measurement of day and night neutrino energy spectrum at SNO and constraints on neutrino mixing parameters*, arXiv:hep-ex/0204009, 2002.

[37] D. A. Green, F. R. Stephenson, *The historical supernovae*, arXiv:astro-ph/0301603, 2003.

[38] M. Turatto, *Classification of supernovae*, arXiv:astro-ph/0301107, 2003.

[39] SK Collaboration, *Search for supernova relic neutrinos at Super-Kamiokande*, arXiv:hep-ex/0209028, 2002.

[40] SNO Collaboration, *SNO and supernovae*, arXiv:astro-ph/0103324, 2001.

[41] DONUT Collaboration, *Observation of tau neutrino interactions*, Physics Letters B 504 (2001) 218-224.

[42] F. R. Paturi, *Chronicle of technology* (in czech), Fortuna Print, Prague, 1992.

[43] H. N. Nelson, *A list of famous physicist photos*, http://hep.ucsb.edu/people/hnn/physicists.html, 1996.

[44] J. Reinhardt, *Picture gallery of famous physicists*, http://www.th.physik.uni-frankfurt.de/~jr/physlist.html, 2002.

[45] The Nobel Prize Internet Archive, *Nobel Prize in Physics Winners 2003-1901*, http://almaz.com/nobel/nobel.html, 2003.